ELSEVIER

In Collaboration with
the Netherlands Institute for Sea Research

JOURNAL OF SEA RESEARCH

Journal of Sea Research 38 (1997) 381–412

Modelling the population dynamics of *Calanus* in the Fair Isle Current off northern Scotland

M. Heath [a,*], W. Robertson [b,1], J. Mardaljevic [a,2], W.S.G. Gurney [b]

[a] *Marine Laboratory Aberdeen, PO Box 101, Victoria Road, Aberdeen, AB11 9DB, UK*
[b] *Department of Statistics and Modelling Science, University of Strathclyde, 26 Richmond Street, Glasgow, G1 1XH, UK*

Received 31 July 1996; accepted 28 July 1997

Abstract

The population dynamics of a marine zooplankton species in the Fair Isle Current off northern Scotland have been investigated by modelling and field study. An age- and weight-structured model of a population of the copepods *Calanus finmarchicus* and *Calanus helgolandicus* was embedded in a biomass based ecosystem model comprising nutrients, phytoplankton, and other non-*Calanus* zooplankton. The model was configured to represent a Lagrangian water column drifting in the Fair Isle Current off the north of Scotland during June 1988, with physical characteristics derived from the results of a three-dimensional hydrodynamic model of the northwest European shelf. The time-series results from the model were compared to data from a semi-synoptic field study by assuming the system to be short-term steady state and transposing the spatially resolved field observations into pseudo-time series along the modelled column drift track. The hydrodynamic model correctly reproduced the general physical characteristics of the system which were destratification of an initially stratified water column as a result of advection through a tidally energetic mixing zone, and subsequent re-establishment of stratification with distance downstream. The biological components of the model were broadly successful at reproducing the main features of the phytoplankton biomass response to the physical processes. The field data indicated that, despite the short-term changes in phytoplankton abundance along the drift track, the stage composition and biomass of the *Calanus* population was relatively stable. However, the model revealed that the main diagnostic features of the response were at the individual level, reflected in the weight at age distribution and reproductive output. The study highlights the difficulty of obtaining adequate data for testing complex models of zooplankton responses to short-term spatio-temporal variations in physical forcing.

Keywords: North Sea; zooplankton; advection; growth; development; ecosystem

1. Introduction

Modelling the short-term responses (less than one month) of zooplankton populations to resource fluctuations is a demanding task. Simple bulk biomass models can rarely capture the key diagnostic features of the response, which is likely to be most strongly reflected in the developmental stage composition of

* Corresponding author. Tel.: +44 1224 295432; Fax: +44 1224 295511; E-mail: heathmr@marlab.ac.uk
[1] Present address: Department of Mathematics and Statistics, University of Lancaster, Lancaster, LA1 4YF, UK.
[2] Present address: Institute of Energy and Sustainable Development, DeMontfort University, The Gateway, Leicester, LE1 9BH, UK.

1385-1101/97/$17.00
PII S1385-1101(97)00047-6

the population rather than in the population biomass. Structured population models of zooplankton species have previously been published (e.g., Carlotti and Nival, 1992; Carlotti et al., 1993; Henderson and Steele, 1995; Steele and Henderson, 1995; Carlotti and Radach, 1996) but coupling to the lower trophic levels and to physical forcing in a way which adequately accounts for both spatial and temporal dynamics has not yet been achieved. Three-dimensionally resolved ecosystem models such as ERSEM (Baretta et al., 1995) typically carry a wide range of state variables at each spatial node, so that modelling the complete nutrient–plankton food web requires compromises in terms of the detail with which any one species or group of species can be represented. The inclusion of age and/or size resolved representations of particular species is potentially very costly in computational terms and therefore problematic for incorporation in a three-dimensionally resolved model. In this study, we develop a Lagrangian water column model to represent the planktonic ecosystem in a parcel of water drifting through the frontal system in the Fair Isle Channel, and embed within this a structured population model of the copepod *Calanus* sp. (representing *Calanus finmarchicus* and *Calanus helgolandicus* which co-occur in the study area). The results are evaluated by reference to data from a dedicated field study. The approach is a compromise on the physical structure which still retains both spatial and temporal characteristics, but which provides a platform for development of the structured population model. The next step (Bryant et al., 1997) will be to simplify the structured population model whilst retaining its essential dynamic properties, to an extent that inclusion in a three-dimensionally resolved scheme becomes feasible.

2. Study background

2.1. General characteristics of the study region

The spatial characteristics of hydrographic fronts in shelf seas are often correlated with distributions of biomass at all trophic levels and frequently coincide with biogeographic boundaries between biological communities (Simpson and Hunter, 1974; Le Fevre, 1986). Often, the observed distributions of biomass can be accounted for in terms of the variation in vertical diffusivity across the front which controls the productivity of autotrophs through the supply of nutrients and the mean irradiance, and hence the supply of resources to heterotrophs (Pingree et al., 1978; Holligan, 1981; Le Fevre, 1986; Tett et al., 1986). However, there is increasing evidence that horizontal transport processes may also play an important role in determining the structure and function of biological communities at fronts (Horne et al., 1989; Mann and Lazier, 1991). The physical mechanisms involved in transport along frontal systems and the associated upwelling have been described (Garrett and Loder, 1981), but the mechanisms of cross-frontal transport are less well understood. Such processes must involve large changes in water column potential energy over relatively short time periods. One area where strong cross-frontal transport has been observed is in the Fair Isle Channel between the Orkney and Shetland Isles off the north of Scotland.

The Orkney and Shetland Islands form part of a ridge extending northwards from the mainland of Scotland parallel to the continental shelf edge (Fig. 1). The area to the west of the ridge, between

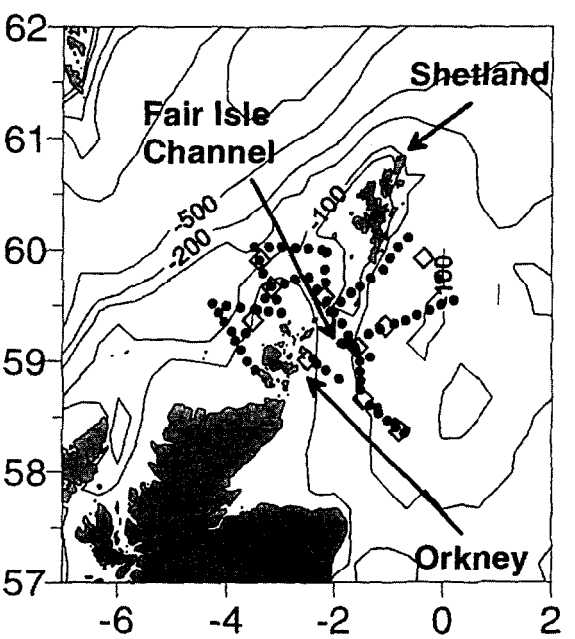

Fig. 1. Location of the Fair Isle Channel in relation to the seabed topography together with standard sampling stations (filled circles) and 'key stations' (open diamonds) where enhanced sampling was carried out during a survey in June 1988.

the islands and the shelf edge, is approximately 100 km wide with water depths of 100 to 200 m. A poleward jet current flows along the shelf edge and warm high salinity water is mixed onto the shelf at various locations. Tidal currents west of the ridge are weak enough to permit seasonal stratification of the water column, although the exposure to wind and wave action causes frequent deep mixing events. East of the ridge, the waters of the northern North Sea basin are subject to intense summer stratification. The ridge itself is punctuated by two gaps. First, the Pentland Firth between Orkney and the Scottish mainland, and secondly the Fair Isle Channel between the Orkney and Shetland Isles. Maximum water depth over the ridge is approximately 90 m and tidal currents across the whole length of the ridge are sufficiently strong that the water column remains mixed throughout the year (Pingree and Griffiths, 1978).

There is a small net residual flow through the Pentland Firth but a strong residual current flows eastwards across the ridge into the North Sea through the Fair Isle Channel, mid-way between Orkney and Shetland. The inflow is composed of water of both Atlantic and Scottish coastal origin. The Atlantic water is drawn from transport across the shelf edge west of Scotland, and the coastal water from inshore areas off the north and west coasts of the mainland. The flow through the Channel has become known as the Fair Isle Current (FIC) (Dooley, 1981, 1983; Turrell et al., 1990). Dooley (1981) noted that during summer months the source waters for the Fair Isle Current are stratified, whilst in the Channel itself the water column is mixed throughout the year. Downstream of the Channel the waters become progressively more stratified with distance into the North Sea. Persistent blooming of phytoplankton was reported on the downstream side of the Fair Isle Channel, and Dooley suggested some relationship between the composition and abundance of algae and the strength of flow through the Fair Isle Channel. Dooley (1981) hypothesised that the basic control of the summer ecosystem in the Fair Isle Channel depends on de-stratification of the water column as the current enters the mixing zone and its subsequent re-stratification as the flow enters the North Sea. The breakdown of stratification on the upstream side of the Channel pumps nutrients from the subsurface layers into the euphotic zone which can then be utilised by autotrophs as the water column restabilises on the downstream side.

The hypothesis of Dooley (1981) was based on field observations of hydrographic and biomass distributions coupled with moored current meter deployments. However, the feasibility of the hypothesised mechanisms and the extent to which any enhanced autotrophic productivity may benefit heterotrophic production has never been quantitatively examined. Such questions are important since the Fair Isle Channel region is ecologically significant as a major seabird breeding area, supported mainly by the production of small planktivorous fish (*Ammodytes marinus*), and for pelagic fisheries (*Clupea harengus*). Against this background, the area is an attractive setting for development and testing of a structured population model of a zooplankton species.

2.2. Sources of data

The modelling work required data as external forcing, for setting initial and boundary conditions, and for evaluation of the results. Physical forcing data were prepared by processing the output from a three-dimensional hydrodynamic model. Chemical and biological initial, boundary and evaluation data were available from a field survey. The principles behind the preparation of data for presentation to the model are described in the following sections. A brief summary of the field data collection is given below.

Field data were collected from MV *Eastella* between 12 and 24 June 1988. The survey was constructed from a series of radial transects centred on the Orkney Isles, each cutting across the core of the Fair Isle Current, and one longitudinal transect down the axis of the Current from west to east (Fig. 1). At each station along the transects hydrographic and chlorophyll fluorescence profiles were collected with a CTD system, surface water samples collected for nutrient analysis (nitrate and nitrite), and depth-integrated mesozooplankton collections carried out with a towed 200-μm mesh plankton net. More detailed sampling was carried out at 10 'key stations' where in addition to the standard sampling, 30 dm^3 water samples from different depth were filtered through 30-μm mesh nets to retain zooplankton, and further water samples preserved intact for the analysis of phytoplankton and microzooplankton, and nutrients

(nitrate and nitrite, ammonium, phosphate and silicate). Vertical profiles of irradiance were measured with a lowered photomultiplier. Also, egg production rate by live female specimens of *Calanus* sp. caught with a vertical haul net was measured in 24-h incubations as described by Hay (1995).

Bulk biomass estimates of phytoplankton (mg chlorophyll m^{-3}) and mesozooplankton (mg C m^{-3}) were derived from the samples collected at all sampling stations. In addition, full taxonomic analyses of the fauna and flora in the samples collected at the ten key stations were carried out, including the developmental stages of the main copepod species. Data from the water samples and the collections made with the various mesh sizes of nets at the key stations were then combined to produce quantitative depth-integrated estimates of the numerical abundance of phyto- and zooplankton species ranging in size from microflagellates of <3 μm diameter to large mesozooplankton (e.g., euphausiids) and larval fish (10–20 mm length). Subsequently, the numerical abundances were converted to species biomass by reference to a database of species mean carbon weights, and all except *C. finmarchicus* and *C. helgolandicus* were aggregated into functional groupings. The two *Calanus* species were treated as a single species (*Calanus* sp.) since they cannot be distinguished by light microscopy in naupliar and immature stages, but retaining the stage resolution of the original data.

3. Modelling approach

As outlined in Section 1, the main incentive for the study was development and testing of a structured population model of *Calanus* sp. capable of simulating the short-term dynamics of abundance in a relatively complex hydrodynamic system. The population model required an environment in which to operate, and this was provided by coupling to a simple nutrient–phytoplankton ecosystem model with the addition of a coarse representation of the other zooplankton competing with *Calanus* for prey. One-dimensional (vertical) implementations of similar models have been developed previously (e.g., Carlotti and Radach, 1996) but in these cases the systems have been forced with physical data representing the temporal dynamics at a fixed (Eulerian) location. Approaches such as these could not easily incorporate the horizontal fluxes of nutrients and biota at any fixed location in the Fair Isle Current which are very significant in relation to the vertical fluxes. Implementing a coupled population and ecosystem model system in a three-dimensional setting capable of simulating these effects would present many difficulties. As a step in this direction, the approach taken here has been to implement a Lagrangian one-dimensional water column model and simulate the temporal dynamics of the biological components as the column is transported through the mixing zone by the Current. The spatial trajectory of the column and the physical conditions within the column (vertically resolved eddy diffusion and temperature) are derived from the output of a three-dimensional Eulerian hydrodynamic model. Hence, the temporal dynamics of the forcing data reflect both regional temporal variations (e.g., seasonality and storm passages) and spatial variations due to the instantaneous geographical location of the column. Exchange between the modelled column and the outside is permitted only at the open deep boundary.

The integrity of the Lagrangian water column approach relies on two main assumptions regarding vertical shear in the model region, and the coherence of the tracked water mass. First, vertical shear is assumed to be negligible. If strong vertical shear is present then the various layers in the initial water column will in reality be advected along very different trajectories and the concept of an intact drifting column will be invalidated. And second, horizontal exchange with water masses of different properties is assumed to be zero. If the streamlines in the region diverge or converge, then this would indicate significant horizontal exchanges between water masses and invalidate the drifting column concept.

Testing of the integrity of these assumptions in the Fair Isle Channel area is described in the following sections.

4. The hydrodynamics of the fair isle current

4.1. Description of the hydrodynamic model

The physical setting for the Lagrangian water column model was provided by the output from a three-dimensional hydrodynamic model (HDM) specifically formulated to predict the temperature stratifica-

tion of the North Sea (Pohlmann, 1996a,b,c,d). The full model domain extended from the shelf edge in the northwest to the continental European coast in the east and included the North Sea region 50°–62°N 5°W–13°E. The Orkney–Shetland region occupied only a small part of this region.

The horizontal node spacing of the HDM was approximately 20 km. The vertical node spacing was devised to have the greatest resolution over the region of thermocline development. The upper 50 m was divided into ten layers of equal thickness whilst below 50 m the layer thickness became progressively greater with depth (10 m, 15 m, 25 m, 50 m, and so on).

The surface forcing parameters for the HDM were temporally resolved sea surface temperature, wind stress and air pressure fields. At the open boundaries of the HDM, the forcing due to the M_2 tide and all other significant far-field effects were provided by a vertically integrated two-dimensional baroclinic model extending westwards into the Atlantic Ocean.

The HDM outputs (three dimensional flow vectors, temperature, salinity, vertical eddy diffusion and Schmidt number at each model node) were provided by the model originators (the Institut für Meereskunde, Hamburg, Germany) at a time resolution of one hour for the years 1988 and 1989.

4.2. Coherence of streamlines in the HDM flow field and column integrity

The first test of water column integrity involved the release of particles from a grid of start points covering the western boundary of the model domain. Particles were launched at fixed depths and tracked until they left the model domain or grounded. This was carried out for a range of depths (layers in the HDM) down to 150 m. Taken layer by layer, the particle trajectories or streamlines derived from the HDM were tightly packed, suggesting the presence of a core current. The origin of the core current was at the western boundary of model domain centred about latitude 59°20′N. The particle trajectories from north and south of this position showed strong divergence from the core streamline bundle suggesting that they represented water masses distinct from the core current. These features were a persistent pattern in the particle trajectories for all but the top layer. The wind-induced horizontal shear occasionally caused the surface Ekman layer (top 5 m of water) trajectories to differ markedly from the pattern observed for deeper layers.

Within the core, the water column is assumed to progress through the channel between Shetland and Orkney without significant dislocation along the column length, i.e. minimal vertical shear. To test the validity of this hypothesis, a number of particles (one at each HDM layer) were released at the core origin. Animation of the ensemble of trajectories revealed that the particles spread out as they progress through the shallowest section of Orkney–Shetland gap. However, the prevailing tendency was for the particles to regroup in deeper water southeast of the gap. Furthermore, the amount of spread was generally not significant compared to the overall length of the trajectory and was mostly along the trajectory path rather than across it.

The final test involved tracking column streamlines as opposed to individual layer streamlines. Here the particles along a line of depth were coupled to form a column. The column was displaced by some average of the individual particle velocities. The details of the weighting scheme for determining the column velocity are described later. For this test, a set of 22 columns were launched from a line of constant longitude (4°24′E) covering the latitude range from 58°42′N to 59°45′N. The columns were started at 01:00 h on 1st May 1988 and tracked for 80 days at the HDM time-step of one hour. The exercise was repeated using the 1989 HDM flow field for the same start time/date. The column trajectories for May–July 1988 are shown in Fig. 2. Note that the column positions are plotted at daily intervals so that the tidal ellipse component of motion does not confuse the overall picture. These trajectories (or streamlines) include a tightly packed bundle of tracks that pass through the gap with little lateral dispersion, revealing the core current in the HDM flow field. A closely similar pattern was present in the 1989 HDM output for the same months. Further tests have demonstrated that the core current is a generally stable feature in the HDM data throughout the years 1988 and 1989; only severe meteorological forcing conditions completely disrupt the streamline bundle.

The dimensions of the tidal ellipse (major axis) traced out by the column-streamlines during each tidal cycle were not constant. The ellipse length min-

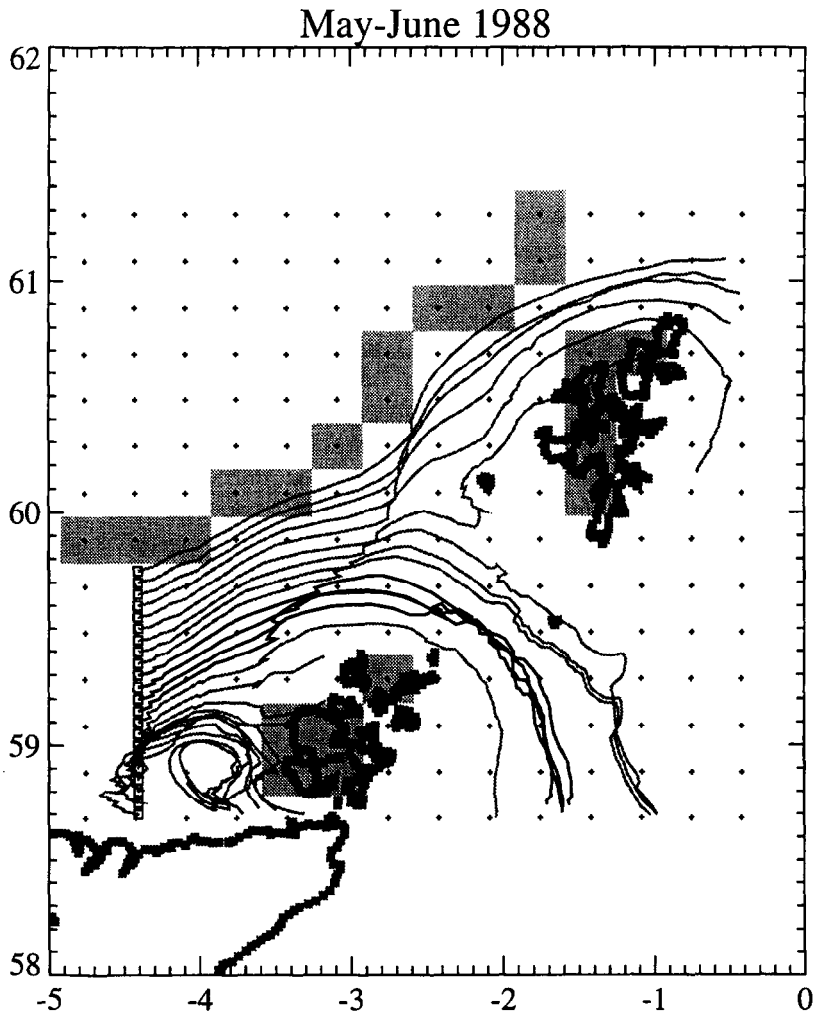

Fig. 2. Trajectories (daily resolution) of columns released along a line of constant longitude on 1 May 1988. Column tracks representing the core of the Fair Isle Current are shown heavy, columns outside the current core are shown faint. Dots indicate the locations of horizontal grid nodes for the subset of data from the North Sea hydrodynamic model. Dry nodes (land) and the boundary to the shelf model are indicated by filled grey boxes.

ima (~2–4 km) were in deep water at the beginning and end of the track. The maximum length of the ellipse was mid-way in the shallowest water where it ranged from ~8–10 km. These dimensions define the scales over which water in the core must be considered to be laterally well mixed. The dimensions of the tidal ellipse (2–10 km) are, however, small when compared to the overall length (without the elliptical excursions) of the trajectory (~250 km).

Taken together, the findings from these tests lend support to the following hypotheses that:

- a core current does exist;
- it is a persistent feature for the majority of weather/forcing scenarios for the years 1988 and 1989;
- the vertical shear in the core current is small compared to the trajectory length; and,
- over small scales the core current is likely to be laterally well mixed.

In conclusion, the sensitivity analyses established the validity of representing the spatial and temporal variability of the physical characteristics of the Fair Isle Current by a Lagrangian water column open only at the bottom boundary. Adopting this approach

greatly simplifies the task of implementing a stage-resolved model of *Calanus* in tandem with a bulk biomass representation of the remaining plankton ecosystem. Details of the calculations required to compile the physical parameters required to force the biological dynamics of the water column model from the HDM data, are described in the following section.

5. The Lagrangian water column system

The requirements of the physical component of the Lagrangian water column system were to derive the geographical position of the column at each time step, and extract from the HDM output the instantaneous values of temperature and vertical eddy diffusion for each depth layer in the column.

5.1. Water column trajectory

The horizontal components of the water column velocity at each model time step were a depth weighted average of the HDM u (east–west) and v (north–south) velocity components at the fixed grid points in the HDM surrounding the instantaneous position of the column. The biological model required that the column length remain constant throughout the simulation. The maximum possible water column length was therefore limited to the minimum seabed depth encountered along the modelled trajectory. It should be noted that the bathymetry of the HDM is itself a smoothed model of the actual bathymetry with a horizontal resolution of ~20 km. A preliminary study was necessary to determine the maximum column length which could pass through the Orkney–Shetland gap under a wide range of conditions without grounding. These exploratory tests revealed that, for a column released at the standard start position, the minimum seabed depth along the track was in the range of 80 to 100 m. Displacing the start position by 5–10 km, or the start time by 14–28 days did not alter these findings. In fact, the column trajectory from the standard start position was found to be stable for the majority of flow regimes in the hydrodynamic model data for 1988 and 1989. The water column length was therefore set to 75 m, which was the lower boundary of the 12th layer in the HDM data. Thus, using the east–west (u) velocities as an example, the horizontal components of the velocity of the column at time t, $u_c(t)$ and $v_c(t)$, were the layer-thickness weighted averages of the layer velocity components along the length of the column:

$$u_c(t) = \frac{\sum_{k=1}^{k=12} u_k(t) d_k}{\sum_{k=1}^{k=12} d_k}$$

where $u_k(t)$ is the u-component of flow velocity at time t for layer k, and d_k is the thickness of layer k.

The HDM velocity field varied considerably in magnitude and direction over distances comparable to the model node separation (~20 km). Also, the HDM bathymetry contains steep gradients to the north of Orkney where the column trajectory passes through the gap; for some adjacent model nodes the bottom depth steps from 30 m to 100 m. The model domain therefore is a highly dynamic system.

Many particle tracking schemes employ a bi-linear interpolation algorithm to determine inter-node parameter values. Bi-linear schemes do, however, possess several drawbacks. Two-stage interpolations make use of only three of the four bounding nodes. Three-stage interpolations give an estimate using all four nodes, but the estimate is sensitive to the design of the scheme for all but degenerate cases, e.g., when the inter-node position is at the exact centre of the four bounding nodes. Both the two- and three-stage bi-linear schemes could therefore introduce a bias in the estimate for inter-node magnitude. A more accurate estimate can be obtained by assuming continuity between the four bounding nodes, i.e. a surface fit interpolation. This was implemented for the particle tracking in the form of a neighbourhood averaging scheme whereby the magnitude at the inter-node position was a weighted average of the values at the four bounding nodes. The weight applied to each bounding node value was proportional to the $1/(\text{distance})^2$ from the inter-node position. Rather than evaluate a set of weights at every unique position in the column trajectory, weights on a fine scale sub-grid were pre-determined and reused throughout the simulation. The weights at the nearest sub-grid node to the actual column position were used in the summation for the average. Tests revealed that a sub-grid 1/20 the dimension of the actual node separation was sufficient — finer scales than this for the sub-grid produced

insignificant changes in the column trajectory. The HDM model node spacing in the east–west direction was latitude dependent, therefore a set of weights were evaluated for every 'row' of model data.

As stated earlier, this region is very compact and the bathymetry gradients steep. A tracking algorithm which does not allow for encounters with a HDM dry node would result in the termination of most tracks mid-way through the Orkney–Shetland gap. The tracking algorithm devised for this particular application permits the column to 'clip' dry nodes. When encountered, a bounding dry node is set to the average of the (bounding) wet node values. The pre-determined weights are then used to evaluate the inter-node value. This strategy for substituting bounding dry node data with estimates is tolerated so long as at least one of the four bounding nodes is wet. This must be so at each of the 12 HDM layers which correspond to the column length. If this condition is not met the trajectory is terminated. Otherwise, the column is tracked until it either leaves the system or reaches a specified maximum age. Note also that this 'clipping' procedure works effectively with the surface fit interpolation algorithm.

The latitude range of the region of interest is fairly small: approximately 3° centred on latitude 60°N. But even here the imposition of a fixed Cartesian co-ordinate system would result in significant displacement errors over the dimensions of the entire region. To avoid this problem, at each time-step the Cartesian xy displacements were converted to latitude-longitude displacements (which include correction for latitude). The xy displacements were evaluated using a simple forward Eulerian method for each of the components u_c and v_c. The track for a column launched from the standard start position (59°20′N 4°30′W) at 01:00 h on the 1st June 1988 is shown in Fig. 3. This is designated the standard June 1988 track — physical forcing parameters were extracted from the HDM for this trajectory.

5.2. Extraction of eddy diffusion and temperatures along column tracks

The travelling column may be visualised as a line in the z-plane which cuts through the four-dimensional space–time data from the hydrodynamic model. The position in time depends on the start date and age of the track and the position in space depends on the track trajectory.

The physical forcing parameters for the biological model were temperature and vertical eddy diffusion. The temperature and eddy diffusion data were predicted by the HDM at the same temporal and spatial resolution as the current velocity components — hourly time-series for every wet node in the model domain. As with the velocity components, inter-node values were estimated using the pre-determined weights evaluated at the sub-grid scale. The temperature and diffusion parameters were extracted from the HDM data field as the tracking simulation progressed.

Even though the method described above produced a very finely resolved spatio-temporal data set for forcing the biological model it was clearly unrealistic to suppose that features on a spatial scale smaller than the node separation in the original HDM were representative of small scale processes. The raw model time–depth data were therefore filtered to remove sub-grid scale 'noise'. This was achieved by means of frequency domain filtering implemented using standard fast Fourier transform library routines. A low-pass filter was applied to the extracted time–depth map layer by layer. The cut-off period for the filter was set to 100 h. This time corresponds to a net horizontal displacement for the column of approximately 20 km, which is equivalent to the HDM horizontal node spacing. The filtering therefore ensures that only those processes commensurate with the grid scale of the HDM persist in the physical forcing time-series for the biological model.

Following the low-pass filtering, the irregular-spaced depth layers were interpolated to a regular grid to be subsampled as necessary to extract forcing data for the biological model (Fig. 4). For this track (June 1988), the bathymetry driven vertical eddy diffusion and the erosion of the thermocline in the shallow section of the trajectory is readily apparent. Tracks for other periods also show storm-driven surface mixing events.

6. The biological model

6.1. Model structure and formulation

The operating environment of the *Calanus* population model was provided by dynamic coupling to

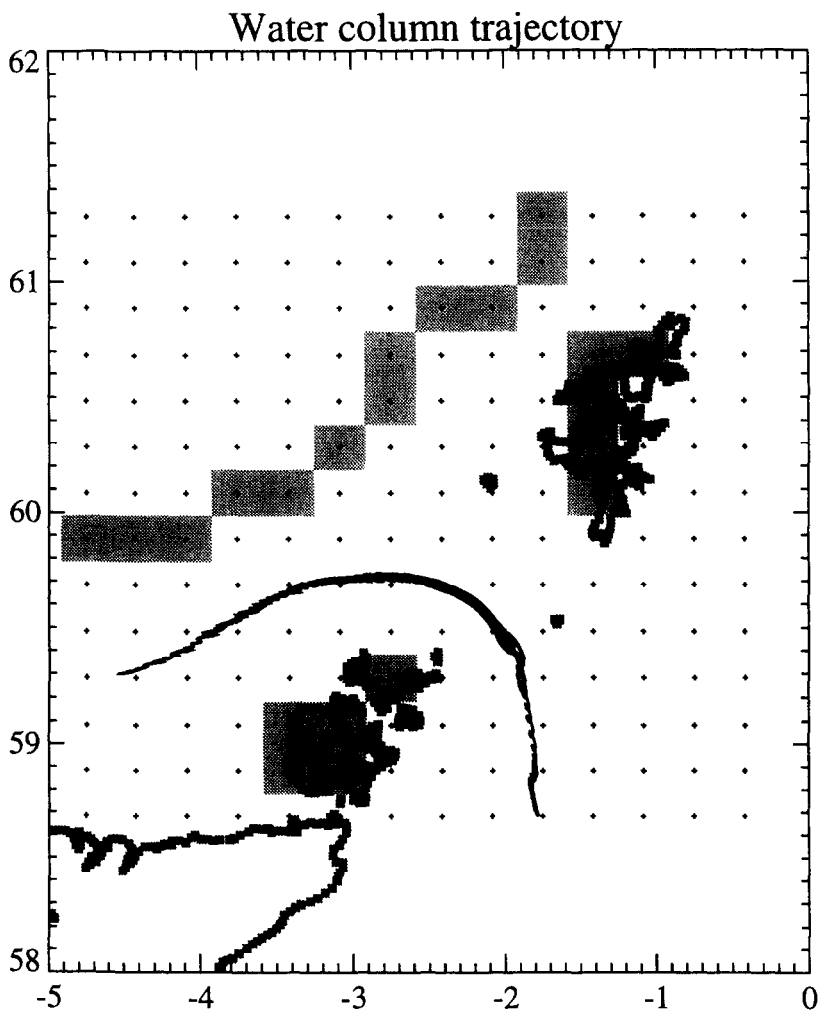

Fig. 3. Definitive track (hourly resolution) of the Lagrangian water column released on 1 June 1988 and used to derive forcing data for the biological model.

an ecosystem model of lower and competing trophic levels. In developing the ecosystem model it was considered important not to loose sight of the overall objective, which was to provide a simulated environment for the model *Calanus* population, and not to develop a comprehensive model of the plankton ecosystem. The ecosystem model was adapted mainly from that published by Ross et al. (1993, 1994) and included six modelled components:

- total dissolved inorganic nitrogen (nitrate, nitrite and ammonium)
- dissolved organic nitrogen
- detrital nitrogen
- nitrogen biomass of two phytoplankton categories representing species with low maximum growth rate, nutrient half saturation constant and sinking rate (notionally flagellates), and species with high values of these parameters (notionally diatoms)
- depth-integrated nitrogen biomass of all non-*Calanus* zooplankton species, including microzooplankton, having a notional depth distribution which adapted to the distribution of prey.

Two phytoplankton groups were included to represent the different species compositions encountered in stratified and vertically mixed waters. From hereon they are referred to as flagellates and diatoms

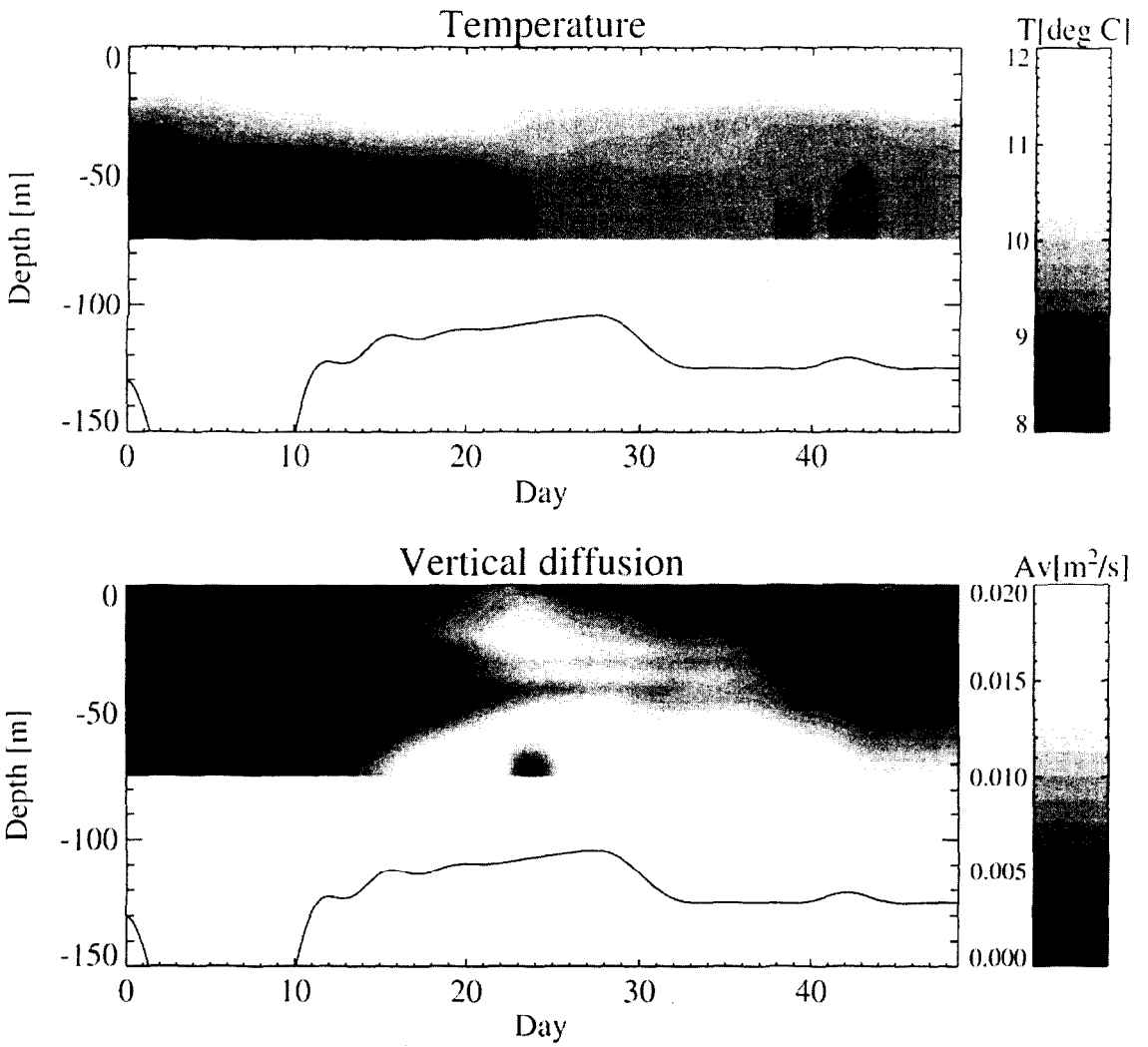

Fig. 4. Low pass filtered time–depth maps of temperature and vertical eddy diffusion interpolated from the physical model to 1 m depth resolution, which formed the physical forcing input to the biological model.

although it is clear that the distinction between the groups is not sufficient to explicitly distinguish these taxa. The non-*Calanus* zooplankton were modelled as herbivores even though the group implicitly includes many omnivores. However, the purpose of including the group was solely to represent the competitive interaction with *Calanus*. In this case the consequence of carnivorous feeding (other than on *Calanus*) is merely to effect an increase in respiration rate and flux to detritus.

The model was implemented in a one-dimensional (vertical) depth-resolved water column with temperature and vertical eddy diffusion coefficients provided as forcing data from the column tracking model. Thus, the time dynamics of the system could be transposed to spatial dynamics along the column trajectory.

The *Calanus* model was constructed as a depth-integrated metapopulation of individuals feeding interactively off the two phytoplankton categories and in return contributing to the pools of dissolved nutrients and detritus. The implicit depth distribution of animals i.e. the depth at which the population fed and returned nutrient and detritus to the ecosys-

tem, was dynamically linked to the modelled depth distribution of prey. The population was constructed as an 'escalator-boxcar train' (De Roos, 1988) of up to 80 age classes each of 1 d width. In this model, individuals were recruited initially as eggs, and moved along the train with time, increasing in weight according to a physiologically based model of ingestion, assimilation and allocation of resources in an individual *Calanus*. Mortality was imposed as a simple function of body weight to mimic the mortality pattern of taxonomic stages. Egg production was modelled for individuals which survived to the age of maturity, as a function of ingestion and body weight. At each output time step the modelled abundance of individuals at age was converted to abundance at taxonomic stage for comparison with field data. This was accomplished by assigning the individuals in each age class to a stage according to the modelled individual weight-at-age and a standard weight range for each stage (Hay et al., 1991; Appendix A, Table A5).

The fact that juvenile stages of *C. finmarchicus* and *C. helgolandicus* could not be discriminated in the field samples used to initialise and test the model presented a conceptual problem for the formulation and parameterisation. The detailed physiological differences between the two species are not well understood, although they seem to related more to temperature than to prey responses, and result in different latitudinal ranges and seasonal patterns of reproduction. The distributions of the species overlap in the Fair Isle area, *C. finmarchicus* having a peak in abundance in the spring, and *C. helgolandicus* in the autumn (Planque and Fromentin, 1996). Unfortunately, many physiological studies reported in the literature do not unequivocally identify which species was being studied (e.g., Thompson, 1982), so it is not possible to produce species-specific parameters for the physiological responses to temperature. Some of the response may be behavioural as reflected in different patterns of vertical distribution in relation to temperature in stratified water columns when the surface temperature exceeds 14°C (Williams, 1985). However, these conditions did not occur in the study area during June 1988. Taken overall there seemed to be no justification for attempting to distinguish between the two species in the model. Thus, the modelled depth distribution of *Calanus* stages was entirely driven by prey abundance considerations, and the temperature dependence of physiological responses was generic.

Mathematically, the ecosystem and *Calanus* models were formulated as a series of coupled ordinary and partial differential equations, all of which are detailed in Appendix A. To solve the equations, the partial differentials were reduce ordinary differentials by applying the 'method of lines' (see for example Al-Rabeh, 1992) and solved with standard techniques for stiff equations (Gear, 1971; Dew and Walsh, 1981). Note that this can in principle be done to any arbitrary level of depth resolution. In practice a resolution of 10 m was applied.

6.2. Initial and boundary conditions for the biological model

Initial conditions for each of the components of the ecosystem model were supplied as vertical profiles of nutrient concentration, diatom, flagellate and non-*Calanus* zooplankton biomass derived from field survey data collected in the area west of Orkney. The initial age composition and abundance of the modelled *Calanus* population was derived from measured stage abundance data by reference to estimates mean stage durations at the observed water temperature taken from the literature (Thompson, 1982; Pederson and Tande, 1992; Miller and Tande, 1993).

The water surface was taken to be a closed boundary in the ecosystem model, so that the flux for all quantities at the surface of the water column was zero. However, the boundary condition at the bottom of the column was more difficult to specify. The tracking model showed that the water depth along a typical streamline decreased to around 75 m as the water column entered the shallow region between Orkney and Shetland, and then gradually increased again on moving into the northern North Sea. Hence, the length of the modelled column must be not more than the water depth at the shallowest part of the track. The column length was set at 75 m and the bottom boundary condition switched between being open or forced when the water depth was greater than 75 m and closed otherwise. The open condition was applied to phytoplankton and detritus, while dissolved inorganic nitrogen (DIN) and dissolved organic nitrogen (DON) were prescribed (outside the

75 m depth region) by time-series of concentrations at 75 m derived from the field survey data.

7. Biological data assimilation

The data from the field survey carried out in June 1988 were processed to establish the initial and boundary concentrations of state variables in the biological model, and to provide time series for comparing with model results. The approach to data processing assumed that the ecosystem was approximately in steady state over the time scales relevant to this study. These time scales were set by the time taken to complete the survey (12 days) and the duration of envisaged model runs (40–50 days). Accepting this assumption, the field measurements at different locations were equated to temporal changes in a column of water travelling through the system. The assumption of steady state is justified by the stability of thermally stratified conditions in the northern North Sea which controls the frontal structures around the Fair Isle Channel. Stratification is intense during mid-summer and other studies have shown that for a period of 1–2 months when the heat flux is at the seasonal maximum, the nutrient–phytoplankton system approaches a steady state (Henderson and Steele, 1995). Thus, the steady state assumption is tenable for the period covered by the field data, but would not be so for other times of year.

The method for converting the semi-synoptic field data to time series was first to interpolate the data at particular depth horizons onto uniform grids covering the study region (58°00′N–60°30′N, 04°30′W–00°30′E, one depth layer per grid) and then to project the surfaces so formed onto the path of the modelled water column. The data were gridded onto a 150 × 150 matrix of nodes (1′ latitude ×2′ longitude or approximately 1.85 × 1.85 km) using an inverse-distance algorithm. The column track was then overlaid onto each grid in turn, and the temperature at the *xy* (longitude, latitude) location corresponding to each hourly interval along the trajectory calculated by interpolation. The accumulated data from each layer were then equivalent to time-dependent profiles of each variable produced by the models. *Calanus* egg production rate, temperature, nitrate plus nitrite, and ammonium data were treated exactly as described above. Some variations were necessary in order to process the phytoplankton and zooplankton abundance data, and these are described in the following sections.

7.1. Phytoplankton abundance and composition

The aim was to produce separate time series for diatom and flagellate groups. The data available were: (1) species-resolved numerical abundance at the 10 key stations, and (2) total chlorophyll at approximately 1 m intervals at the 70 or so standard stations (including key stations). To maximise the amount of information extracted from these data, both sets were combined, thus obtaining high spatial resolution from the standard station data and species resolution from the key stations.

Time series of chlorophyll concentration in each 10 m depth layer were produced exactly as for temperature, and converted to carbon using a carbon : chlorophyll ratio of 30 mg C/mg Chl (Riemann et al., 1989). The proportional contributions of diatoms and flagellates to the depth-integrated phytoplankton biomass at the 10 key stations was then calculated, gridded and projected onto the column track. Diatoms constituted <10% of the biomass at the beginning and end of the track, and up to 50% in the middle region. Finally, these proportions were applied to the total carbon biomass in each layer to obtain the time series for each phytoplankton group at 10 m depth intervals.

7.2. Zooplankton abundance and composition

In the case of zooplankton data the problem was to dissect the total biomass into that attributable to each developmental stage of *Calanus* sp., and that due to all other zooplankton. As with the phytoplankton, detailed taxonomically resolved information was available at the key stations only, and more general data (total depth-averaged mesozooplankton biomass) from the spatially extensive standard sampling. The procedure was as follows:

A time series for the depth-integrated total mesozooplankton biomass was produced by gridding and interpolation. The proportion of depth-integrated biomass accounted for by *Calanus* sp. (all stages) at the key stations was then calculated from the taxonomic data and likewise gridded and projected. The

product of these two time series then provided separate series for both *Calanus* sp. and non-*Calanus* mesozooplankton biomass along the column track. Next, the *Calanus* sp. stage composition data at each key station were used to estimate the proportional contribution of each stage to the total *Calanus* sp. biomass. These proportions were then gridded and projected. Finally, the time series of *Calanus* sp. biomass was apportioned to stages and converted to numbers of individuals using average weight-at-stage data (Hay et al., 1991; Appendix A, Table A5).

It remained to add microzooplankton biomass to the non-*Calanus* mesozooplankton time series to produce a series for all non-*Calanus* zooplankton. This was achieved by griding of depth-averaged microzooplankton data from the key stations and projecting onto the column track in the usual way. The results were then added to those for non-*Calanus* mesozooplankton biomass derived earlier.

7.3. Summary of the observed data

The temperature time series synthesised from the field data is in accordance with the hypothesised physical effects occurring along the column path and compared well with the results from the hydrodynamic model. Initially stratified conditions were broken down in the Fair Isle Channel, and re-established on the downstream side. The data showed an increase in depth-integrated chlorophyll corresponding to passage through the well-mixed region. At the same time nutrients were mixed upwards towards the surface and phytoplankton mixed downwards out of the photic zone. Flagellates dominated the phytoplankton population in the stratified waters, and diatoms dominated in the mixed region. This was in accord with the principle that flagellates have a competitive advantage in stratified waters since they sink only slowly, while diatoms are generally able to compete more effectively in mixed waters where redistribution due to vertical mixing overrides the effects of sinking (Joint, 1987).

Adult *Calanus* (C6) numbers were roughly constant throughout. If the steady state assumption is accepted then this implies that adult mortality must have been broadly in line with the rate of promotion from C5. Egg numbers were especially low, and nauplii and C1 numbers were also low, in the early part of the track. Eggs and nauplii increased rapidly after 23 and 37 days, respectively (see Section 8). There are some apparent inconsistencies in these data: (1) the increase in egg abundance at day 23, together with the fact that the average duration of the egg stage was less than two days at in-situ temperatures, suggests that there should have been be a corresponding increase in nauplii numbers around day 25, not day 37 as observed; and (2) there were apparently no eggs at all prior to day 10, yet there were significant numbers of nauplii before this time. These discrepancies most likely reflect the sparse nature of the original data on eggs and nauplii which was based only on the 30 dm^3 water samples from the ten key stations. The copepodite stage C1 and older abundances were based on both water and towed net samples which contained many more individuals. Similarly, the observed rates of egg production by female *Calanus* were highest (approximately 23 eggs $female^{-1}$ day^{-1}) during the early part of the track and declined with passage through the mixing zone (see Section 8), which was inconsistent with the absence of eggs from the water column in the upstream area and the increasing abundance with distance along the track. In view of these uncertainties, specification of the stage abundance of *Calanus* population at the start of the track for use as initial conditions in the model was problematic. The solution was to accept the copepodite abundance data as being reasonably robust, but to extrapolate the time series for eggs and nauplii back from the more stable abundances in the mid-part of the track to produce estimates of numbers at the start.

8. Model results

In the following sections, results from the default configuration of the model are presented, followed by those from a refined configuration including adjustments to the physical forcing.

8.1. Default model results

Vertical eddy diffusion data from the water column tracking model are shown, for completeness, in Fig. 5, and predicted DIN and phytoplankton in Figs. 6 and 7.

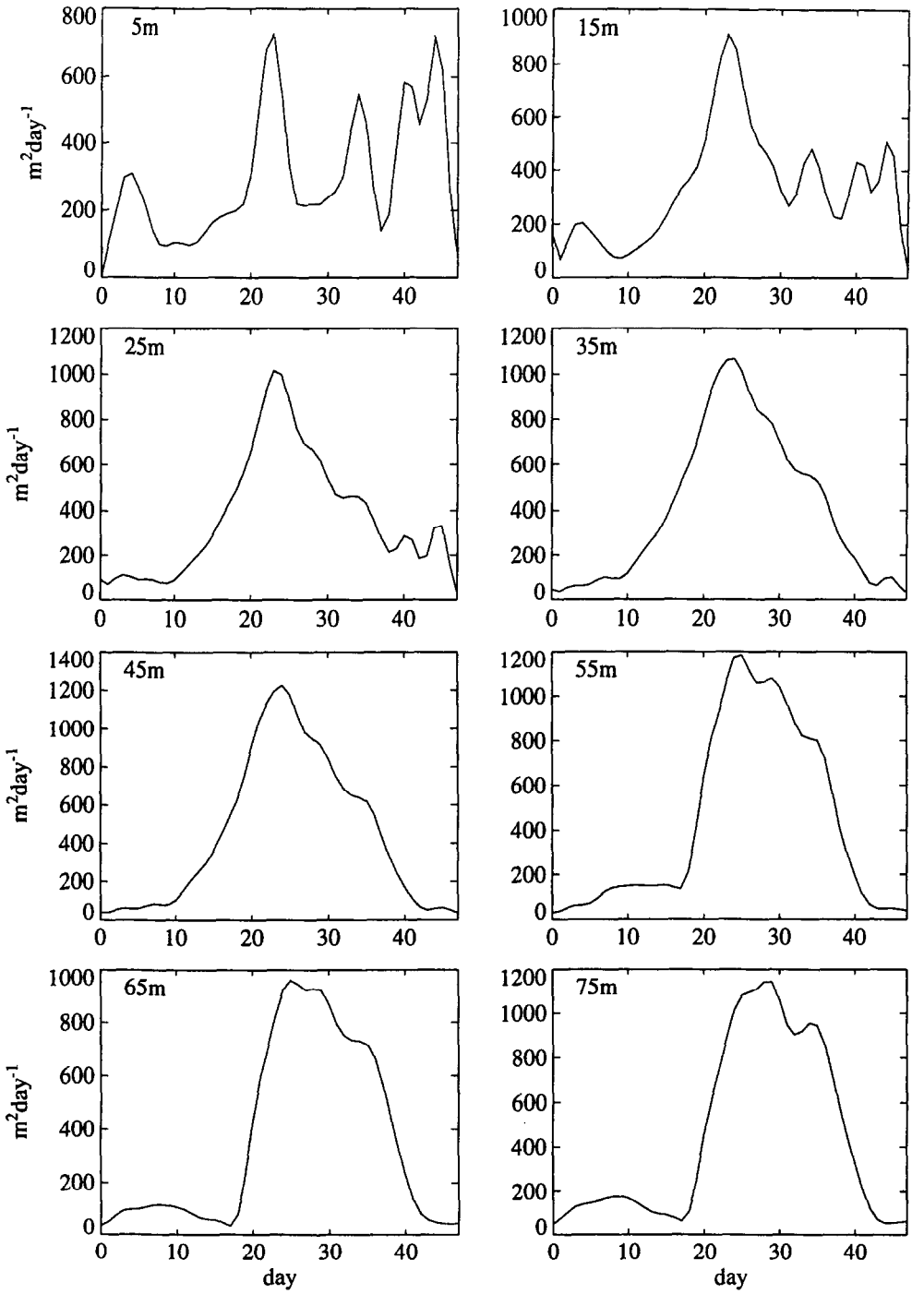

Fig. 5. Default time series of vertical eddy diffusion at each depth horizon derived from the Lagrangian water column system.

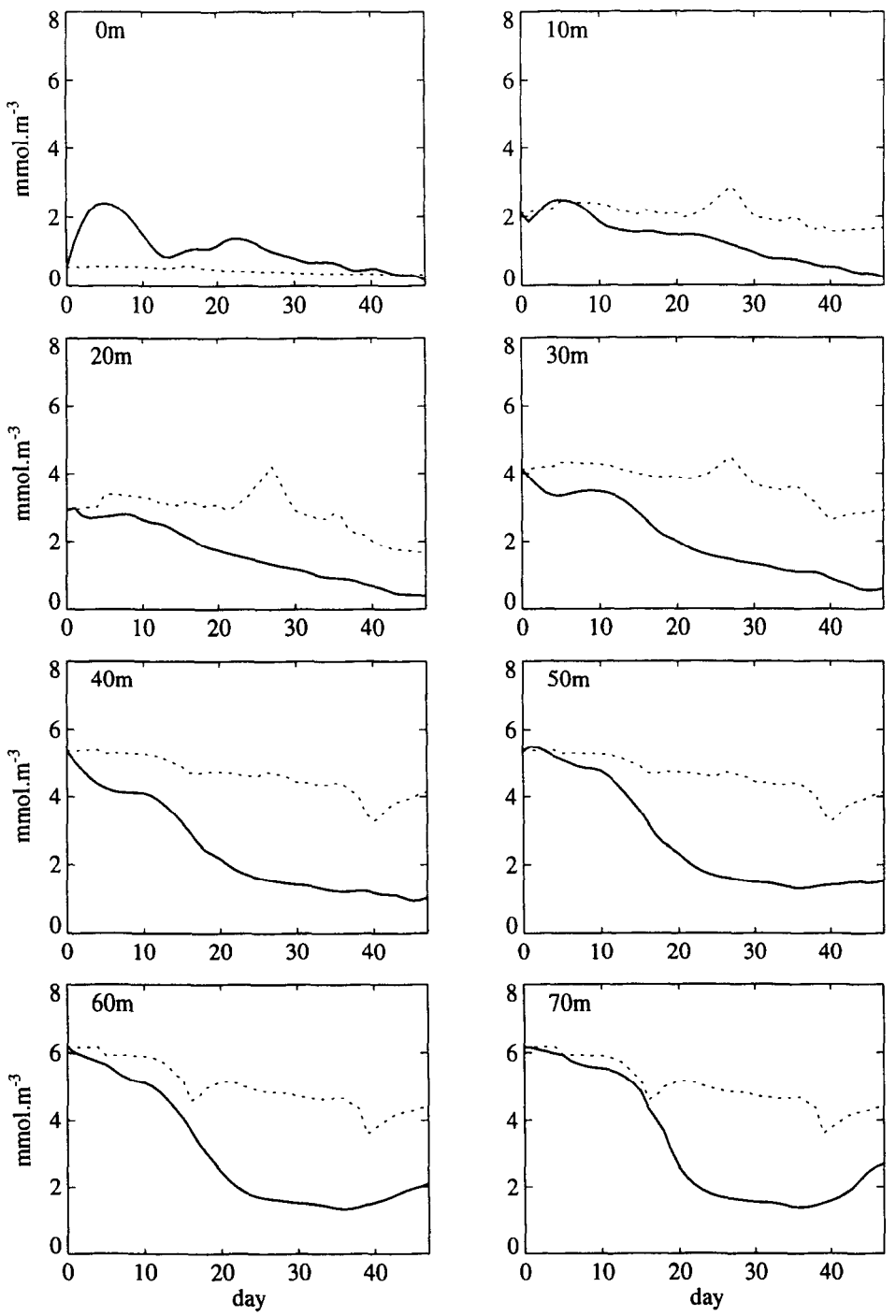

Fig. 6. Modelled (continuous) and observed (dotted) time series of DIN at each depth horizon using the default forcing data on vertical eddy diffusion.

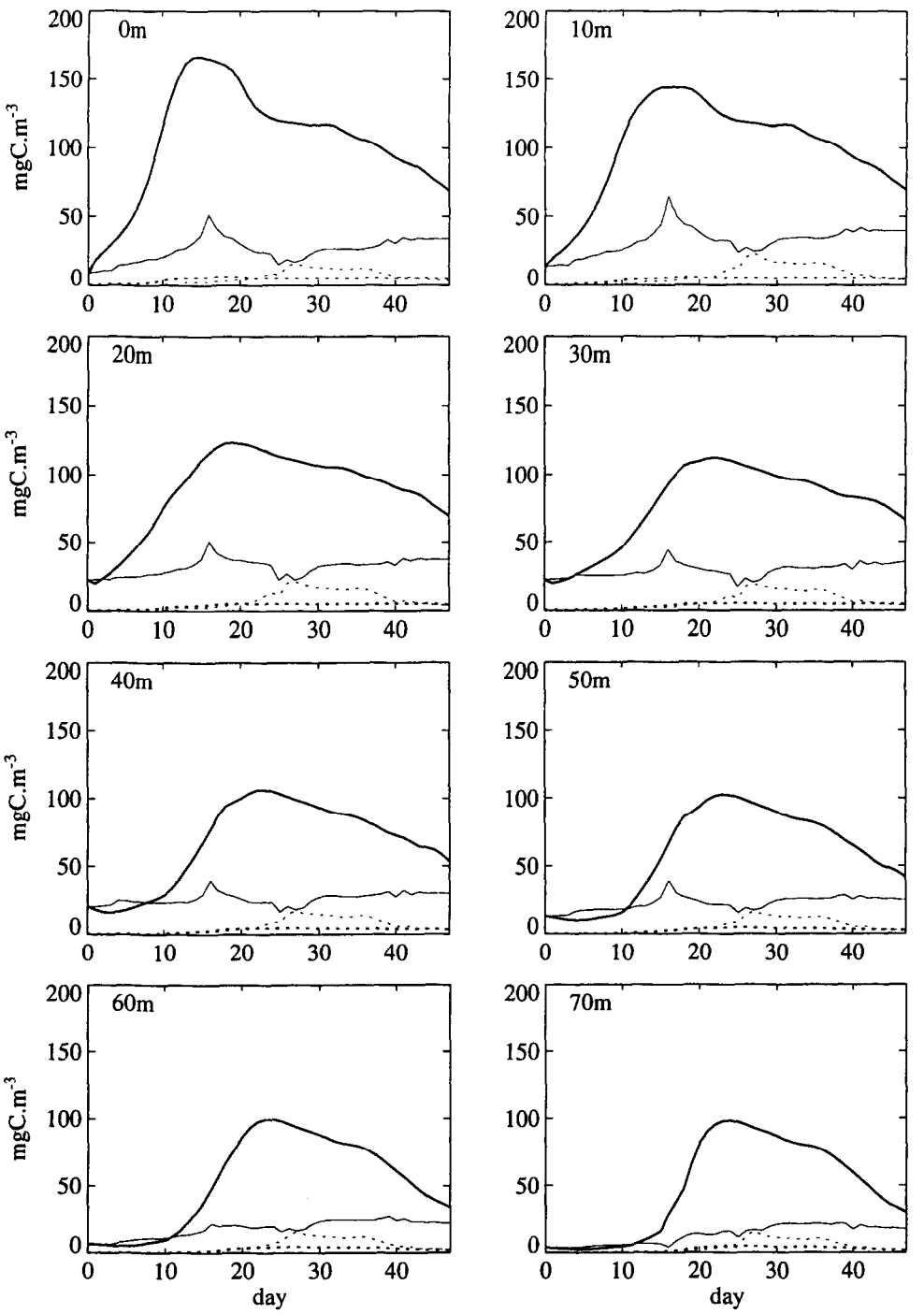

Fig. 7. Modelled (bold) and observed (faint) time series of diatom (dotted) and flagellate (solid) carbon biomass at each depth horizon using the default forcing data on vertical eddy diffusion.

DIN concentrations (Fig. 6) were over-predicted in the surface layer and under-predicted elsewhere. Note that the only feature in the observed data sufficiently pronounced as to not be attributable to noise was the fall in concentration after 10 days below 50 m; this was greatly overstated in the model predictions.

Flagellates (Fig. 7) dominated throughout, and were greatly over-predicted except towards the bottom of the column in the first part of the track.

Extensive sensitivity analysis of biological parameters, in particular the phytoplankton irradiance and nutrient uptake parameters, showed that the values which would be required to reconcile the model performance in the upper layers with the observations would be orders of magnitude outside the range of published values. The physical forcing data were therefore investigated for an explanation of the large discrepancy between the default model results and the observations. Returning to the observed DIN concentration data along the particle track in Fig. 6, consider in particular the differences between concentration at the surface and at 10 m. The concentration gradient of around 0.15 mmol m^{-1} was maintained throughout, despite the high eddy diffusion rates predicted by the hydrodynamic model. Smaller, but still significant, gradients occurred between 10 and 20 m and between 20 and 30 m. A simple first order calculation shows that, for a typical value (300 m^2 d^{-1}) of the eddy diffusion at 5 m in the forcing series, maintenance of the observed 0–10 m DIN concentration gradient would require gross primary productivity to be in the order of 500 mg C m^{-3} d^{-1}, i.e. 5 g C m^{-2} d^{-1} in the upper 10 m of the water column alone. This is clearly unrealistic. For example, Wood et al. (1973) estimated annual average gross annual primary production to be only 0.2 g Cm^{-2} d^{-1} in the top 10 m of an irradiance-limited system in a Scottish sea-loch. The raw nutrient data were carefully checked, but no evidence could be found of systematic bias between measurements at 4 m for the routine stations and in subsurface samples from the key stations which could provide an explanation. It was concluded that the eddy diffusion rates in the surface layer of the HDM were higher than could be sustained by the observed nutrient and phytoplankton data. A similar conclusion was drawn from an investigation of the performance of a water column implementation of the ERSEM model forced by the same physical data (I. Allen, ERSEM project document 10/9/95).

8.2. *Refined model results*

A resolution of the inconsistency between the eddy diffusion rates and the observed data was accomplished by scaling the predicted values of the eddy diffusion at 5 m by a constant amount, and in the absence of measured data this scaling factor was treated as a fitting parameter. Similarly, the eddy diffusion rates at 15 and 25 m were reduced by (other) constant amounts. No other model parameters were changed during this process. Reduction of the eddy diffusion rates at 5, 15, 25 m by factors of 75, 25, 5 respectively was found to result in more reasonable behaviour of the nutrient–primary producer system — the remainder of the results presented in this section are calculated with this modification in place.

DIN concentrations (Fig. 8) were now somewhat under-predicted in the surface layer, but extremely close to the observed data elsewhere.

Phytoplankton results are shown in Fig. 9. Note firstly the sharp peak in observed flagellates at around 15 days. Examination of the horizontal distribution of nitrate and chlorophyll in the surface waters indicates that this was a consequence of a small-scale, localised upwelling of nutrients in this region. Since the phenomenon occurred on too small a scale to be resolved by the hydrodynamic model (20 km node spacing) it could not be represented in the vertical mixing rate driving data and there was therefore no mechanism by which the model presented here could reproduce this feature.

Flagellates were again over-predicted in the upper two depth layers, though by no means to the same extent as in Fig. 7. The model matched the data at the remaining depths reasonably well. Diatoms were, however, uniformly under-predicted at all depths and the decline in diatom abundance towards the end of the model run was not reproduced.

'Other' zooplankton (Fig. 10) were over-predicted by around 25% — this was a result of the over-prediction of (total) phytoplankton in the depth layers in which they were most abundant. The results of the structured *Calanus* model portrayed two main cohorts maturing and reproducing during transit of

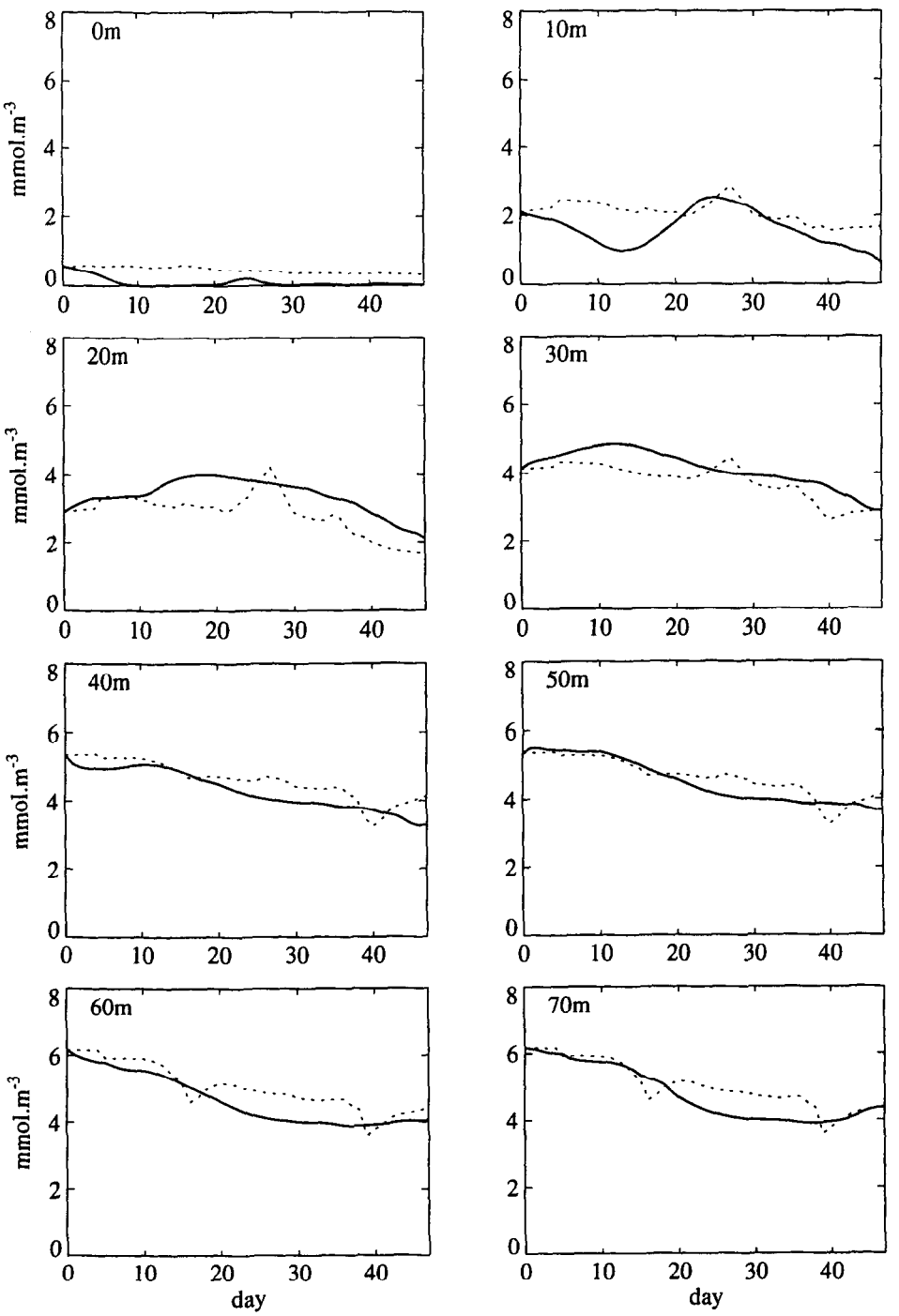

Fig. 8. Modelled (continuous) and observed (dotted) time series of DIN at each depth horizon using the refined forcing data on vertical eddy diffusion.

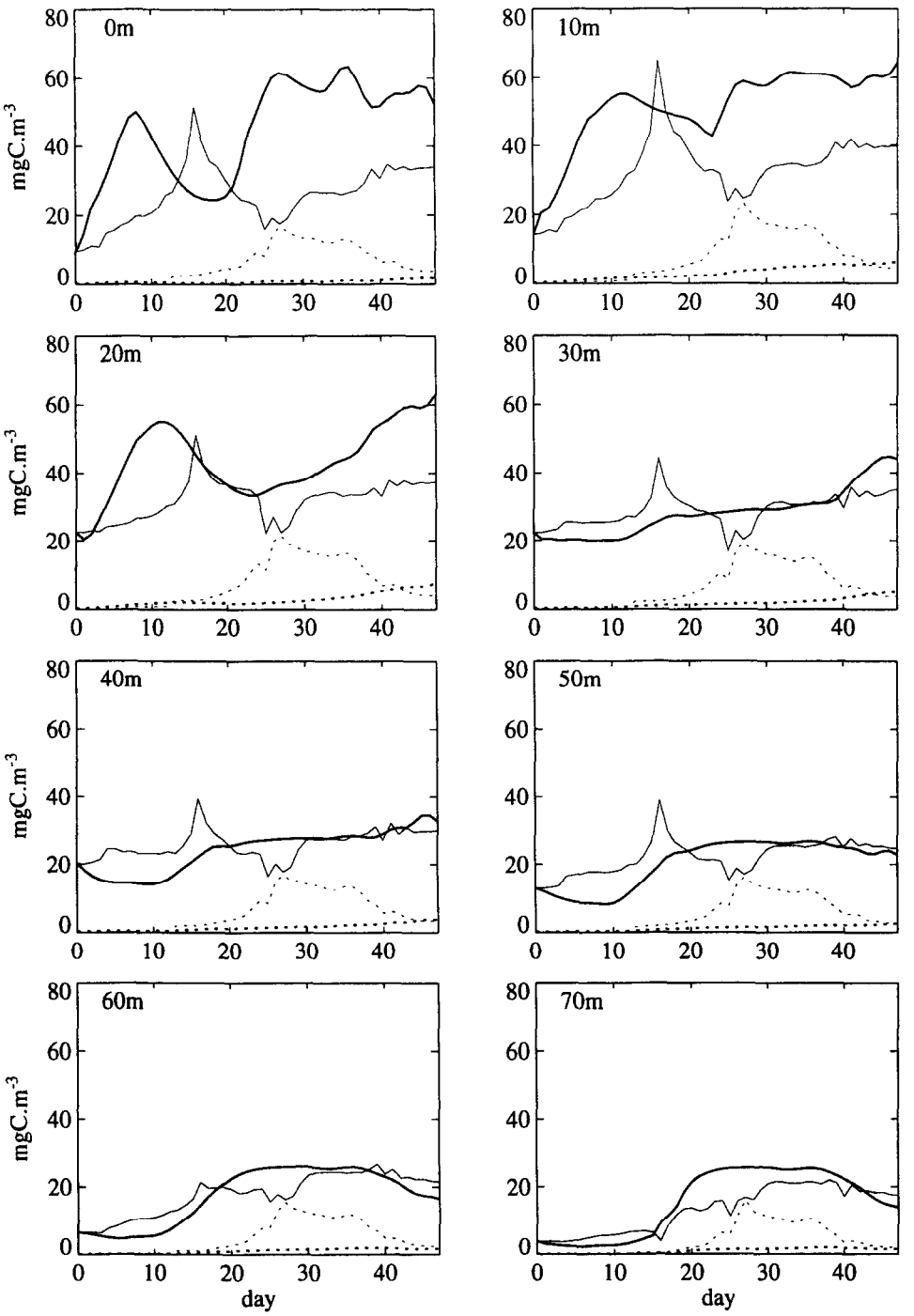

Fig. 9. Modelled (bold) and observed (faint) time series of diatom (dotted) and flagellate (solid) carbon biomass at each depth horizon using the refined forcing data on vertical eddy diffusion.

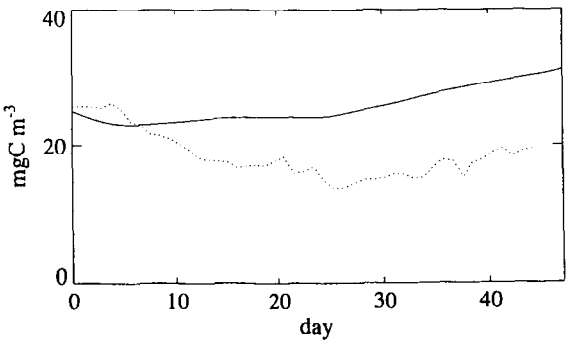

Fig. 10. Modelled (bold) and observed (dotted) data on non-*Calanus* zooplankton carbon biomass.

the Fair Isle Channel (Fig. 11). The first cohort was present in the initial conditions as immature stages C4 and C5, which matured and spawned around days 10–20. The resulting eggs attained stage C4–C5 by the end of the model run, with a few individual reaching C6 and initiating a further wave of spawning. It is extremely difficult to discern discrete cohorts propagating through time in the observed data. This is almost certainly because the original data were not in fact a time series but a semi-synoptic map along the drift track which has been converted to a time series by assuming a stable equilibrium over the time scale of the column trajectory. Nevertheless, it can be concluded that the actual *Calanus* population was stable along the trajectory, there being no evidence of significant decline in any of the stages, and this property was reproduced by the model. It should be emphasised that maintaining a roughly constant population through time whilst supporting reproduction and growth is by no means the default behaviour for sensitive models of this type.

Investigation of the individual weight at age results for the modelled *Calanus* population (Fig. 12) revealed that individual weight at age decreased, or in other words stage duration as specified by a weight interval increased, during the first 20 days of the simulation and then remained relatively constant. The conclusion is that modelled phytoplankton abundance in the early part of the track was insufficient to sustain the initial weight at age distribution, but the increased production on entering the mixing zone in the Fair Isle Channel redressed this situation. No spatially resolved field data on *Calanus* weight-at-stage were available for comparison with the model results, but the study clearly demonstrates the diagnostic potential of such information.

The ratio of egg numbers : C6 numbers in the modelled population (Fig. 13) reflected the gamete production rate. Since the modelled egg stage duration was 2 days and the daily egg mortality rate was 0.9, then the average residence time of an individual egg stage was approximately 1.1 d. Hence the ratio egg numbers : C6 numbers was within 10% of the egg production rate per C6. The ratio remained low during the first 20 days of the simulation (<10 eggs/C6), but increased sharply to >20 eggs/C6 around day 25–30 and then declined to 7 eggs/C6 by the end of the run. These results differ markedly from the ratio eggs : C6 in the observed population which, as described earlier, contained inconsistencies in egg numbers in the early stages of the track, but showed some agreement with the direct measurements of egg production by *Calanus* females in bottle incubations carried out aboard the ship. The observed rates agreed closely with the modelled stage ratio from day 20 onwards. However, on the upstream side of the Channel (day 0–20), measured egg production per female was relatively higher than the modelled stage ratio. The reasons for this discrepancy are far from clear since the observed phytoplankton concentration on the upstream part of the track agreed well with the model and seems insufficient to support the observed egg production rates. One possible explanation could be that on the upstream side of the Channel the *Calanus* were feeding on other zooplankton as well as on phytoplankton, whilst this feeding link is not present in the model.

9. Discussion

9.1. General strategy

The work described combines both spatial and temporal components of physical variability into the dynamics of a water column model. The focus is on the population dynamics of a single species (*Calanus*) which is explicitly represented in the model, but in an ecosystem context. We explicitly account for the entire biomass of other species competing with, and forming a resource for *Calanus*, but at a lower taxonomic resolution as a platform to support the explicit population model. A La-

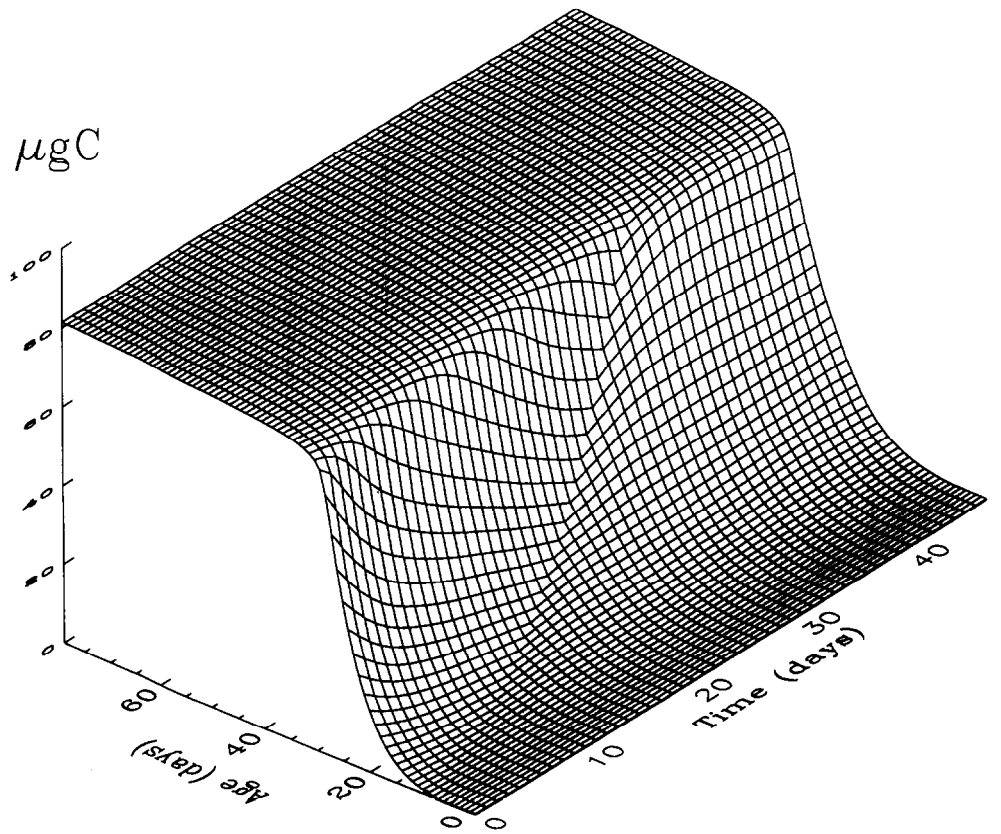

Fig. 12. Modelled time series of individual weight at age in the *Calanus* sp. population along the column track.

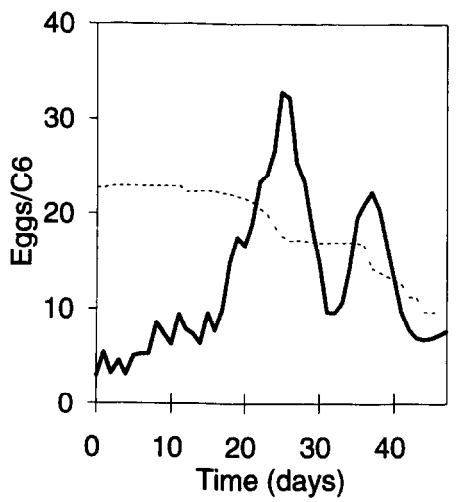

Fig. 13. Modelled time series of the ratio of egg numbers to C6 numbers (continuous), together with the observed (dotted) time series of egg production (female^{-1} d^{-1}) produced by projecting gridded data on egg production rates measured at sea onto the column track.

grangian rather than a more conventional Eulerian three-dimensional modelling approach was chosen in this case to circumvent the need to represent horizontal mixing exchanges of *Calanus* individuals. The latter would have required holding the entire age and weight structure at each node in the model, with attendant overheads on computation costs. There are precedents for the Lagrangian approach (e.g., Woods and Onken, 1982; Wolf and Woods, 1988; Woods and Barkmann, 1995), but few if any involving the explicit representation of a particular species in dynamic competition with the rest of the ecosystem.

The field data available to this study were comprehensive in terms of their taxonomic and spatial resolution, but we were forced to make assumptions of steady state in order to synthesise Lagrangian temporal dynamics from the data. Other studies have relied on Eulerian data with superior temporal resolution, but poor or no spatial dimension (e.g., modelling of the FLEX studies by Henderson and Steele, 1995). In

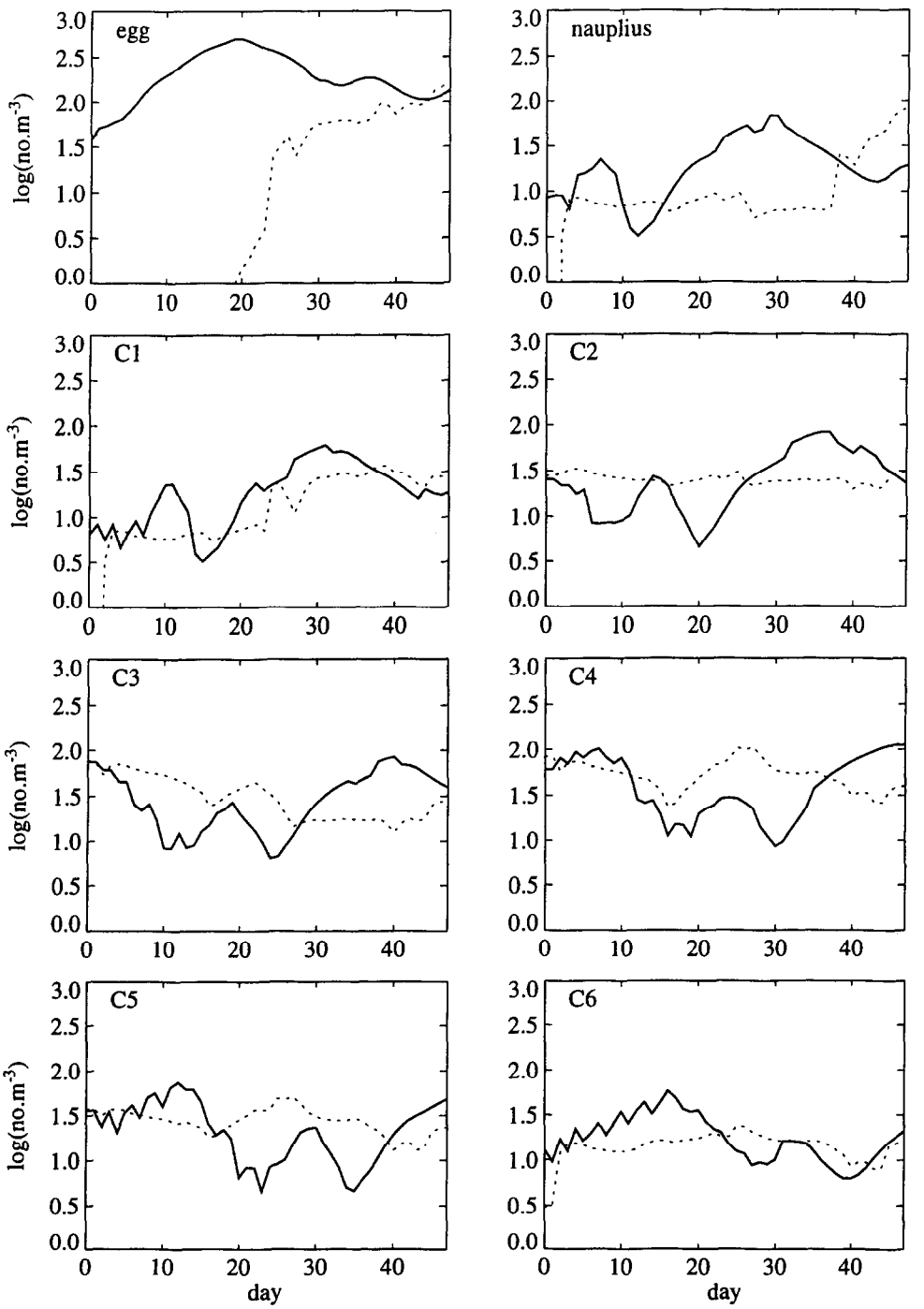

Fig. 11. Modelled (bold) and observed (dotted) time series of *Calanus* sp. numbers in stage in the water column. Model run using the refined forcing data on vertical eddy diffusion.

reality, neither situation is entirely satisfactory. In the former case, the spatial distribution of state variables was almost certainly not in steady state on the time scale of the drift trajectory of our water column in the Fair Isle Current, so that our inferred time series data could not be a completely accurate representation of the evolution of a drifting water column. In the latter case (FLEX), it is almost certain that horizontal transport must have contaminated the time series signals at the Eulerian sampling station. The solution would appear to be a tracking study based on time series sampling close to a drifting marker or a dye tracer patch. However, such approaches also have attendant problems of accounting for vertical shear and patch diffusion. The maximum practicable duration for such studies in shelf seas appears to be 10–15 days, being limited by the extent to which drifting markers may deviate from the movements of the surrounding water in tidally energetic areas or dye patches remain identifiable. Nevertheless, a long duration tracking study with comprehensive time series sampling, carried out in a strongly varying physical environment or at a dynamic time in the seasonal cycle, could provide a strong basis for future modelling.

9.2. *Physics–nutrient–phytoplankton model*

The modelled nutrient–phytoplankton system was intentionally simplified in several respects. Inorganic nutrients were represented only by DIN, there was no explicit representation of the microbial food web, and phytoplankton were represented only by two competing groups (nominally diatoms and flagellates). This minimal representation of the lower trophic levels, compared to for example the ERSEM model (Baretta et al., 1995) was adopted in order to minimise the degrees of freedom in the parameter space outside the main focus of interest which in this case was *Calanus*. It was necessary only that the modelled lower trophic levels broadly reproduced the spatial and temporal dynamics of the total phytoplankton biomass with a minimum of parameter fitting. The nutrient–phytoplankton model was successful in achieving this, although not without the introduction of fitting parameters to scale the vertical eddy diffusion rates in the upper three layers of the water column. The main discrepancy was in relation to diatoms which were consistently under predicted by the model. The functional differences between the modelled diatom and flagellate categories were solely in the nutrient half-saturation constant, maximum growth rate and sinking rate, but adjustment of these parameters within acceptable ranges would probably not resolve the discrepancies. Initial investigation suggests that the key lies in the prey preferences of the modelled *Calanus* and other non-*Calanus* zooplankton. As presently implemented, neither group shows any preference for diatoms over flagellates, which means that the zooplankton groups respond only to the total phytoplankton abundance. This was intentional, to simplify the parameter space and focus attention on the structured *Calanus* model. However, in future developments we would introduce differential grazing of the diatoms and flagellates by the zooplankton.

Despite extensive investigation, it was not possible to reconcile the eddy diffusion rates in the upper 30 m of the water column derived from the HDM with the observed data on vertical distributions of DIN and phytoplankton biomass. The observations alone suggest that the HDM eddy diffusion rates were excessive, but the reasons are not clear. The values produced by the HDM at 5 m depth were around 200 to 300 $m^2\ d^{-1}$ during the period when the column was stratified which according to the equation of Davies (1986) should be equivalent to a wind speed of approximately 2.5 $m\ s^{-1}$. Reduction of the eddy diffusion rate by the fitting factor of 75 only changes the estimated wind speed to around 0.5 $m\ s^{-1}$, which is still consistent with the calm weather conditions which prevailed during the field survey. HDM eddy diffusion rates at 5 m towards the middle of the track, where the column entered the tidal mixing zone, were higher (1000 $m^2\ d^{-1}$), and from this point onwards the observed temperature gradient in the upper 10 m of the water column was steeper than that predicted by the model suggesting that the propagation of bottom-generated mixing towards the surface was overestimated in the model. This is an acknowledged area of uncertainty in physical modelling of shelf seas (Soulsby, 1990; Henderson and Steele, 1996). Further extensive analysis of the vertical eddy diffusion rates produced by the model has been presented by Pohlmann (1996b).

Another contributory factor may be the nature of the thermal forcing of the HDM. The heat in-

put forcing of the HDM was provided by gridded sea surface temperature data at 14-d intervals, rather than by heat flux data (Pohlmann, 1996b). Temporal dynamics in vertical structure and eddy diffusion rates in the model were a response to changes in surface temperature and wind stress. However, there was no attempt at temporal smoothing of the surface temperature data so that the time variations at any geographical location showed high frequency fluctuations superimposed on a sinusoidal seasonal cycle, which may not be realistic. During 14-d periods when the forcing data implied net heating of the surface waters, the model responded by predicting intensification of stratification and reduced eddy diffusion rates. Conversely, during periods of implied surface cooling the model responded by increasing the eddy diffusion to generate a heat flux into the deeper layers even under constant wind stress. Thus it is conceivable that forcing the HDM with noisy surface temperature data may have contaminated the short-term dynamics of vertical eddy diffusion in the upper layers of the modelled water column. It is possible that this may have contributed to the internal inconsistencies encountered in our study.

9.3. *Calanus* population model

The attraction of explicitly modelling the population structure of zooplankton species is that stage composition appears to be a more robust indicator of population status than biomass alone (Steele and Henderson, 1993). However, it is clearly meaningless to model the entire zooplankton community on this basis as if it were a single species, hence the approach we have taken in modelling one species explicitly, and the remaining members of the community as a bulk biomass group. This 'twin-track' approach is necessary to correctly simulate the community grazing impact. The lower trophic levels must be modelled dynamically if it is believed that the main species of interest has the capacity to deplete its food resource, and/or suitable phytoplankton forcing data are not available. In our study, *Calanus* represented around 20% of the zooplankton community biomass. Forcing the *Calanus* population model with the observed time series of chlorophyll produced qualitatively similar results to the dynamic version, but at other times of year *Calanus* can constitute up to 70% of the biomass and under these circumstances the dynamic interaction with the phytoplankton system should be more important.

Close examination of the field data on the population composition of *Calanus* sp. revealed some internal inconsistencies with respect to the abundances of eggs and nauplii. These almost certainly reflected the difficulty in obtaining quantitatively comparable estimates of the numbers of both the eggs and early stages, and the adult stages of copepod species in the same population. The differences in individual size and typical concentration mean that a single sampling device is rarely suitable. Usually, as in this study, it is necessary to sample the population with a range of mesh sizes and sample volumes and then attempt to combine the data into an integrated population structure. Nevertheless, an important conclusion of the study is that quantitative sampling of eggs and nauplii, as well as the more easily collected copepodites, is essential for interpreting the population dynamics of species. Furthermore, the model results indicate that the immediate signatures of the *Calanus* response to the enhanced autotrophic production in the Fair Isle Channel were at the individual level in terms of weight-at-stage and reproductive output, rather than the population level. Such observations are not usually available from field studies to the same resolution as biomass data since they are extremely time consuming to obtain. However, more effort needs to be devoted to these measurements to support studies such as this.

An important point to emerge from the development of the *Calanus* model was the need for better taxonomic precision in field and laboratory studies of zooplankton. The inability to distinguish between juvenile stages *C. finmarchicus* and *C. helgolandicus* led to conceptual difficulties in formulating the individual model. In June, when this study took place, water temperatures should be increasing towards the point where reproduction of *C. helgolandicus* is favoured over that of *C. finmarchicus*. However, there are few quantitative data available to parameterise such a distinction between the species, and in any case, the eggs, nauplii and early copepodites could not be distinguished in the field samples. Unfortunately, the two species were not discriminated as C5 and adults in either the net samples or the egg production experiments in this study. In future

studies, this aspect should be given careful attention to provide at least some indication of the validity of modelling the whole *Calanus* population as a single unit.

9.4. Overall conclusions

In conclusion, the study has confirmed the feasibility of the hypothesis proposed by Dooley (1981) for the physical forcing of the nutrient–phytoplankton ecosystem in the Fair Isle Current. The zooplankton system, however, is shown to be more complicated than first imagined, and the physiological ability of individuals to respond to the rapid fluctuations in autotrophic production is of key importance. Better field data than currently exist will be required to unequivocally determine the consequences of the physics of the Fair Isle Current for the propagation of carbon and nutrients up the pelagic food web. Particular points to emerge regarding the conduct of future field studies are (1) the desirability of data from time series sampling at drifting locations, (2) the need to quantitatively sample egg and naupliar stages of zooplankton as well as copepodites, (3) the need for more individually based physiological data, and (4) the need for improvements in the precision of taxonomic identification of individuals in both field and laboratory studies.

Acknowledgements

We especially thank Dr Thomas Pohlmann and Dr Hermann Lenhart at the Institut für Meereskunde, University of Hamburg for performing special runs of the hydrodynamic model and making the hourly data available to us. We also thank our colleagues Niall Broekhuizen, Alejandro Gallego and Steve Hay who made significant contributions in the form of prototype modelling and data analysis. The work was partly funded by a grant from the European Union Marine Science and Technology Programme, contract number MAS2-CT92-0032.

Appendix A. Model formulation

A.1. The Ecosystem Model

The model comprises six dynamic components and a connection to the separate model of *Calanus* sp.:

Component	Symbol
Dissolved inorganic nitrogen (DIN)	N
Dissolved organic nitrogen (DON)	D
Detrital nitrogen	R
'Diatom' nitrogen	P_D
'Flagellate' nitrogen	P_F
Non-*Calanus* zooplankton nitrogen	O
Coupling to *Calanus* model	Z (subscripted)

A.2. Nutrient–phytoplankton system

A.2.1. Rate equations

The one-dimensional water column has a surface z_0 and maximum depth z_{max}. The rates of change of each of the nutrient and phytoplankton categories given depth-dependent diffusivity $K(z)$ and vertical advection rates v_{P_D}, v_{P_F}, v_R for diatoms, flagellates and detritus respectively, are:

$$\frac{\partial N}{\partial t} = \frac{\partial}{\partial z}\left(K(z)\frac{\partial N}{\partial z}\right) + B_D + B_R + E_{O_D} + E_{Z_D} - U_{P_D} - U_{P_F} \quad (1)$$

$$\frac{\partial P_D}{\partial t} = \frac{\partial}{\partial z}\left(K(z)\frac{\partial P_D}{\partial z}\right) - \frac{\partial}{\partial z}\left(v_{P_D}(z)P_D(z)\right) + U_{P_D} - E_{P_D} - I_{P_D} - M_{P_D} \quad (2)$$

$$\frac{\partial P_F}{\partial t} = \frac{\partial}{\partial z}\left(K(z)\frac{\partial P_F}{\partial z}\right) - \frac{\partial}{\partial z}\left(v_{P_F}(z)P_F(z)\right) + U_{P_F} - E_{P_F} - I_{P_F} - M_{P_F} \quad (3)$$

$$\frac{\partial D}{\partial t} = \frac{\partial}{\partial z}\left(K(z)\frac{\partial D}{\partial z}\right) + E_{P_D} + E_{P_F} + E_{O_N} + E_{Z_N} - B_D \quad (4)$$

$$\frac{\partial R}{\partial t} = \frac{\partial}{\partial z}\left(K(z)\frac{\partial R}{\partial z}\right) - \frac{\partial}{\partial z}\left(v_R(z)R(z)\right) + J_Z + lM_Z + M_{P_D} + M_{P_F} - B_R \quad (5)$$

where B_D represents bacterial remineralisation of DON, B_R decomposition of organic detritus to DIN, and U_P the rates of uptake of DIN by diatoms ($P = P_D$) and flagellates ($P = P_F$). I_P, similarly, is grazing of zooplankton on phytoplankton, and M_P is lysis. E is excretion, with the subscripts P_D, P_F, Z_D, O_D denoting the source: phytoplankton are assumed to excrete DON, and zooplankton (Z, O) both DIN and DON. J_Z represents *Calanus* faeces production, M_Z is zooplankton mortality rate, and l the proportion of zooplankton tissue which is readily decomposed (i.e. non-skeletal).

A.2.2. Boundary conditions

The water surface is taken to be a closed boundary, so the flux for all quantities N, P_D, P_F, D, R at the surface of the water

column is zero. Hence for all $t \geq 0$ and with P representing P_D or P_F, then $z = z_0$ and,

$$\frac{\partial N(z,t)}{\partial z} = 0 \tag{6}$$

$$K(z,t)\frac{\partial P(z,t)}{\partial z} - v_P(z,t)P(z,t) = 0 \tag{7}$$

$$\frac{\partial D(z,t)}{\partial z} = 0 \tag{8}$$

$$K(z,t)\frac{\partial R(z,t)}{\partial z} - v_R(z,t)R(z,t) = 0 \tag{9}$$

The bottom boundary may be open or closed depending on the depth of water beneath the column (open or forced bottom boundary condition when the water depth is greater than 75 m and a closed boundary otherwise). The open condition is applied to phytoplankton and detritus, while DIN and DON are prescribed (outside the 75 m depth region) by a time-series of concentration at 75 m, $F_N(t)$, $F_D(t)$. Thus, if t_1 represents the time at which the depth shallows to 75 m and t_2 that at which it increases beyond 75 m again, for $z = z_{max}$ and $t < t_1$ or $t > t_2$,

$$N(z,t) = F_N(t) \tag{10}$$

$$P(z,t) = 0 \tag{11}$$

$$D(z,t) = F_D(t) \tag{12}$$

$$R(z,t) = 0 \tag{13}$$

while for $t_1 \leq t \leq t_2$, Eqs. 6–9 apply with $z = z_{max}$.

A.2.3. Irradiance and nutrient limitations

Both the phytoplankton categories are assumed to have fixed carbon : nitrogen ratios (q) and the uptake of nutrient is governed in a multiplicative manner by irradiance (ι) and dissolved nutrient concentration (N) given by:

$$U_P(z,t) = f_{\theta,P}P(z,t)U_{P,\max}\frac{\iota(z,t)}{\iota(z,t)+K_{P,\iota}}\frac{N(z,t)}{N(z,t)+K_{P,N}} \tag{14}$$

The depth profile of irradiance follows Lambert-Beer,

$$\iota(z,t) = \iota_0(t)e^{-\int_{z_0}^{z}\kappa dz} \tag{15}$$

The surface irradiance, $\iota_0(t)$ is taken from a time series derived for the region by Pätsch (1994), and the attenuation coefficient κ takes the form

$$\kappa = \kappa_0 + \kappa_1(P_D + P_F) \tag{16}$$

where κ_0 is the background attenuation coefficient and κ_1 accounts for self-shading by phytoplankton, with the same coefficient applying to both functional groups. The coefficients κ_0 and κ_1 were calculated from the observed vertical profiles of irradiance and chlorophyll at each of the ten key stations.

The term $f_{\theta,P}$ reflects temperature dependence for P_D, P_F, for which a Q_{10} relationship is applied,

$$f_{\theta,P} = Q_{10,P}^{(\theta-\theta_{0,P})/10} \tag{17}$$

A.2.4. Fluxes to detritus, dissolved pools and zooplankton

Following Ross et al. (1993), it is assumed that phytoplankton excretion is of the form

$$E_P(P,z,t) = x_{u,P}U_P + f_{\theta,P}x_P P \tag{18}$$

and that $x_{u,P}$ and x_P are constant for each phytoplankton group, so ignoring time- and space-dependence of mortality and excretion rates. Similarly, decomposition of detritus and remineralisation of DON are also assumed to be first-order, with constants r and d respectively:

$$B_R(R,z,t) = f_{\theta,B}rR, \quad B_D(D,z,t) = f_{\theta,B}dD \tag{19}$$

with (cf. phytoplankton temperature dependence)

$$f_{\theta,B} = Q_{10,B}^{(\theta-\theta_{0,B})/10} \tag{20}$$

Both diatoms and flagellates are ingested by zooplankton. In the absence of good data on preferential feeding, it is assumed that phytoplankton are taken up in proportion to their relative abundance, so if I_Z and I_O represent total uptake of phytoplankton by *Calanus* and 'other' zooplankton respectively then

$$I_{P_D} = \frac{P_D}{P_D + P_F}(I_Z + I_O) \tag{21}$$

$$I_{P_F} = \frac{P_F}{P_D + P_F}(I_Z + I_O) \tag{22}$$

For simplicity, vertical advection rates v_{P_D}, v_{P_F}, v_R are assumed to be constant, neglecting the effect of phytoplankton nutrient status on sinking rate and the fact that 'detritus' is an aggregation of variously-sized components. The diffusion coefficient K and temperature θ are the time- and depth-dependent driving functions.

Zooplankton faeces and skeletal remains are assumed to be refractory and therefore not remineralised on the timescales considered here. This undecomposed material is integrated over depth and accumulated in a supplementary variable A:

$$\frac{dA}{dt} = \int_{z_0}^{z_{max}}(J_Z + (1-l)M_Z)dz \tag{23}$$

$$A_0 = 0 \tag{24}$$

A.3. Non-Calanus zooplankton

Non-*Calanus* zooplankton ('Other Zooplankton') are represented as a single lumped nitrogen biomass, O, with a depth distribution $p_O(z)$ which follows that of the adult *Calanus* (see later),

$$\frac{dO}{dt} = I_O - E_O - M_O \tag{25}$$

$$O(t=0) = O_0 \tag{26}$$

where I_O, E_O, M_O represent depth-integrated uptake of (all) phytoplankton, excretion, and mortality, and take the forms

$$I_O(t) = \int_{z_0}^{z_{max}} f_{\theta,O}(z)p_O(z)O(t)I_{O,\max}\frac{P(z)}{P(z)+K_{O,P}}dz \tag{27}$$

$$E_O(t) = b_O O(t) + s_O I_O(t) \tag{28}$$

$$M_O(t) = m_O O(t)\left(1 + \frac{O(t)}{O_{\text{ref}}}\right) \tag{29}$$

where $P \equiv P_D + P_F$. Note that the form of the expression for E_O is intended to represent the sum of basal metabolism (b_o) and specific dynamic activity (s_o).

A.4. The Calanus model

Description of the *Calanus* model is in two parts. First, the 'Individual Model' which is concerned with the growth, and reproduction of an individual animal through its life from egg to senescent adult, and second, the 'Population Model' which deals with the age demography and number of individuals in the population.

A.4.1. Individual Calanus model

The Individual Model accounts for both carbon and nitrogen fluxes, and variable names are labelled with subscript C or N accordingly. It is assumed that an individual is characterised by its carbon-weight ω_C, and that it maintains a fixed N : C ratio, so $\omega_N = q_Z \omega_C$.

A.4.1.1 Ingestion

The relationship between an individual's ingestion rate I and the local abundance of food $F(F_N = P_D + P_F,\ F_C = F_N/q_P)$ is given by a type II functional response, characterised by a search volume V and a handling time T, both of which scale as powers of the individual's weight:

$$I_C = \frac{V F_C}{1 + V T F_C} \tag{30}$$

$$I_N = \frac{F_N}{F_C} I_C \tag{31}$$

$$V(\omega) = v_0 \omega^{v_1} \tag{32}$$

$$T(\omega) = \tau_0 \omega^{\tau_1} \tag{33}$$

(The subscript C on ω is omitted for clarity).

Of the ingested material, a fraction f is lost as faeces, and a fraction x is lost as dissolved material through cell lysis etc. Thus, the assimilation efficiency ε is given by

$$\varepsilon_C = 1 - f_C - x_C \tag{34}$$

$$\varepsilon_N = 1 - f_N - x_N \tag{35}$$

defecation (J) and excretion (E) rates are

$$J_C = f_C I_C,\quad J_N = f_N I_N \tag{36}$$

$$E_C = x_C I_C,\quad E_N = x_N I_N \tag{37}$$

and the rate U at which material enters the body proper is

$$U_C = \varepsilon_C I_C \tag{38}$$

$$U_N = \varepsilon_N I_N \tag{39}$$

A.4.1.2 Metabolism

Metabolic losses are assumed to be due to three distinct processes:

(1) Basal metabolism (b), associated with tissue maintenance and background swimming activity
(2) Specific dynamic action (s), associated with digestion and synthesis of new tissues
(3) 'Reproductive Action' (r), associated with the production of gametes etc.

The weight-specific proportionate losses of carbon and nitrogen through metabolism may differ (by a factor α), but it is assumed that the extent to which they differ is the same for basal, activity and specific dynamic action costs. The proportionate nitrogen cost associated with gamete production may be rather higher since gametes are typically protein rich. Following Carlotti and Sciandra (1989) and Carlotti and Radach (1996) it is assumed that basal metabolism is a constant fraction of body weight. Following Marshall and Orr (1958), the temperature dependence is assumed to be exponential, so

$$b_C = Q_{10,B}\exp((\theta - 10)/\theta_B)\beta_0 \omega \tag{40}$$

$$b_N = \alpha q_Z b_C \tag{41}$$

Kiørboe et al. (1985) conclude that specific dynamic action is proportional to the ingestion rate. Hence, the terms for carbon and nitrogen respectively are represented as:

$$s_C = \beta_S I_C \exp\left(-\rho \frac{I_N}{q_Z I_C}\right) \tag{42}$$

$$s_N = \alpha q_Z s_C \tag{43}$$

Similarly, the carbon and nitrogen costs of gamete synthesis are assumed to be proportional (factor γ) to the mass of gametes produced Γ,

$$r_C = \gamma_C \Gamma_C \tag{44}$$

$$r_N = \gamma_N \Gamma_N \tag{45}$$

The net quantity of material available for growth and/or gamete production is then given by

$$N_C = U_C - b_C - s_C \tag{46}$$

$$N_N = U_N - b_N - s_N \tag{47}$$

A.4.1.3 Allocation

After meeting its metabolic demands, any remaining assimilate is partitioned between somatic growth and gamete production. It is assumed that the fractional allocation to gamete production $\Pi(\omega)$ is an increasing function of weight, taking the form of the Dirac-Fermi function (Blakemore, 1987):

$$\Pi(\omega) = \left\{1 + \exp\left(\frac{\omega_\pi - \omega}{\sigma}\right)\right\}^{-1} \tag{48}$$

where ω_π is the weight at which 50% of net assimilate is committed to gamete production and σ specifies the slope of the function at this point.

The carbon costs of reproduction are assumed proportional (factor γ_C) to the carbon weight of the gametes, and nitrogen costs are assumed proportional (γ_N) to the nitrogen weight of the gametes produced. It is assumed that there are no further costs involved in somatic growth (these costs are paid in SDA).

Since, in the model, the animals maintain a fixed N : C ratio, then an individual can grow (or produce gametes) only at the rate determined by the more limiting of the two elements. The condition $q_Z\gamma_C < \gamma_N$ implies that carbon is the limiting element for growth, and $q_Z\gamma_C/(1+\gamma_C) < \gamma_N/(1+\gamma_N)$ implies carbon is the limiting element for gamete production, so the rate of gamete production Γ is:

$$\Gamma_C = \frac{\Pi(\omega)N_C^+}{1+\gamma_C}, \quad \Gamma_N = \frac{q_Z\Pi(\omega)N_C^+}{1+\gamma_C} \quad \text{if C is limiting} \tag{49}$$

$$\Gamma_C = \frac{\Pi(\omega)N_N^+}{q_Z(1+\gamma_N)}, \quad \Gamma_N = \frac{\Pi(\omega)N_N^+}{1+\gamma_N} \quad \text{if N is limiting} \tag{50}$$

Now, the net rate of change in body carbon and nitrogen associated with feeding, metabolism and reproduction can be calculated. Since the animals have a fixed internal quota of nitrogen to carbon, the model requires one final step: that of eliminating the excess, λ, of whichever element has been consumed in excess of the quantity in which it can be utilised. Up to this point, the net change in body weight Δ is

$$\Delta_C = N_C - r_C \tag{51}$$

$$\Delta_N = N_N - r_N \tag{52}$$

and it is required that

$$\frac{\Delta_N - \lambda_N}{\Delta_C - \lambda_C} = q_Z \tag{53}$$

so carbon is limiting if $\Delta_N/\Delta_C > q_Z$ and nitrogen otherwise, and

$$\lambda_C = 0, \quad \lambda_N = \Delta_N - q_Z\Delta_C \quad \text{if C is limiting} \tag{54}$$

$$\lambda_C = \Delta_C - \frac{\Delta_N}{q_Z}, \quad \lambda_N = 0 \quad \text{if N is limiting} \tag{55}$$

Finally the growth rate G of the *Calanus* may be written as

$$G = \begin{cases} \Delta_C - \lambda_C & \text{for feeding stages} \\ G_0 & \text{for non-feeding stages} \end{cases} \tag{56}$$

A.4.1.4 Mortality

Zooplankton mortality rates are notoriously difficult to measure and appear to be highly variable in time and space, even for a single developmental stage (e.g. Wood and Nisbet, 1991). Mortality appears to be highest in the egg stage and adult phase, but little is known about the actual magnitude of the per capita mortality rates. Accordingly, we apply a simple scheme in which per capita mortality rates $D(\omega)$ are assumed to be constant within each stage, and assume zero mortality for all stages except eggs and C6. In the absence of any data, mortality rates of eggs and C6 are treated as fitting parameters.

A.4.2. Calanus population model

The starting point for the population model is the McKendrick–von Foerster equation as applied to the *Calanus* population density Z at time t and weight ω,

$$\frac{\partial Z}{\partial t} + \frac{\partial}{\partial \omega}(GZ) + \delta Z = 0 \tag{57}$$

with the boundary condition that

$$G(t, \omega_e, P)Z(t, \omega_e) = \int_{\omega_0}^{\infty} \beta(t, \omega, P)Z(t, \omega)\mathrm{d}\omega \tag{58}$$

where ω_e is recruitment weight, and initial condition

$$Z(0, \omega) = Z_0(\omega) \tag{59}$$

The population fecundity β is given by:

$$\beta = \frac{\Gamma_C}{\omega_e} \tag{60}$$

The functions G, δ, β represent the per capita growth, mortality and reproduction rates respectively of an individual *Calanus* of weight ω under phytoplankton density P.

The equation is solved by the 'escalator-boxcar train' (EBT) method of solution, described in De Roos (1988). In the terminology of de Roos, the system is restricted to a one-dimensional i-state space Ω bounded on the left by ω_0. The system is further simplified by allowing only a fixed number of cohorts in the EBT scheme, discarding the oldest (after checking that it is 'empty') each time a new one is created, and by considering only a second order scheme.

$Z_j(t)$ is defined to be the number of individuals remaining at time t of those which were recruited during time-interval j, and B_j is their total biomass. Note that the mean individual weight in each interval can be recovered as $\omega_j = B_j/Z_j$.

Applying the EBT method, simplified as described above, to equations Eqs. 57–59 results in the following system of ordinary differential equations:for each time interval Δ_j, $j = 1, \ldots, m$

$$\frac{\mathrm{d}Z_j}{\mathrm{d}t} = R_j - \delta_j Z_j \tag{61}$$

$$\frac{\mathrm{d}B_j}{\mathrm{d}t} = \omega_e R_j + G_j Z_j - \delta_j B_j \tag{62}$$

where

$$R_j = \begin{cases} \sum_k \beta_k Z_k, & j = 1 \\ 0, & j > 1 \end{cases} \tag{63}$$

In order to avoid the computational complexity and cost of solving two-dimensional pde's, the depth distribution of animals is implicit. The individual *Calanus* is envisaged as being 'clockwork', spending a prescribed proportion of time in each depth layer. The depth-dependent distribution function $p(z)$ represents the proportion of time an individual spends in the depth layer $z_{i-1/2} < z < z_{i+1/2}$. In this particular study p is set to 1.0 for the depth layer with the highest phytoplankton concentration and zero elsewhere, thereby maximising the food availability for the animals.

The growth rate G will depend on the phytoplankton density P and the individual weight ω. In particular, the ingestion rate

$I = I(P, \omega)$ of phytoplankton by an individual *Calanus* of weight ω will be depth-dependent through the dependence on P. Writing $I_z(z, t)$ for the total uptake of phytoplankton by *Calanus* of all weights at depth z and time t, then

$$I_Z(z, t) = \sum_j I_N(z, \omega_j) Z(\omega_j, t) p(z, \omega_j) \quad (64)$$

where $I_N(P, \omega)$ is the form of the individual uptake function. Note that I_N must be expressed in terms of N mass. Similarly, the total depth-specific excretion rate E_Z is given by

$$E_Z(z, t) = \sum_j E_N(z, \omega_j) Z(\omega_j, t) p(z, \omega_j) \quad (65)$$

with E_N the excretion by an individual of weight ω. Depth-specific faeces production J_z is

$$J_Z(z, t) = \sum_j J_N(z, \omega_j) Z(\omega_j, t) p(z, \omega_j) \quad (66)$$

and depth-specific contribution to detritus-N due to mortality M_Z is

$$M_Z(z, t) = \sum_j D_N(z, \omega_j) Z(\omega_j, t) p(z, \omega_j) \quad (67)$$

D_N is obtained from the product of per-capita mortality rate $D(z, \omega)$ and N-mass ω_N.

Weight-specific depth-integrated growth, mortality and reproduction rates, G_j, δ_j and β_j are given by

$$G_j \equiv G(t, \omega_j, P) = \int_{z_0}^{z_{max}} G(z, \omega_j) p(z, \omega_j) dz \quad (68)$$

$$\delta_j \equiv \delta(t, \omega_j, P) = \int_{z_0}^{z_{max}} D(z, \omega_j) p(z, \omega_j) dz \quad (69)$$

$$\beta_j \equiv \beta(t, \omega_j, P) = \int_{z_0}^{z_{max}} \frac{1}{\omega_e} \Gamma_C(z, \omega_j) p(z, \omega_j) dz \quad (70)$$

Finally, since the field data on *Calanus* abundances are classified by development stages rather than weight or age, it is necessary to convert model results from number-in-age-class to number-in-stage. At each output interval we assign each age class to a development stage according to the modelled individual weight and a standard weight for each stage (Table A5). The number of individuals in each stage is then obtained by summing over all corresponding age-classes.

A.5. Parameters

Parameters for the phytoplankton, dissolved and particulate organic material, *Calanus* and non-*Calanus* zooplankton groups are given in Tables A1–5. Note that diatom parameters are largely from Ross et al. (1993); corresponding flagellate parameters are obtained from these by scaling according to the same factors used by Varela et al. (1995).

Table A1
Phytoplankton parameters

Parameter	Description	Value	Units	Source
q	C : N ratio	7	mg C (mg N)$^{-1}$	Ross et al., 1993
c	C : Chl ratio	30	mg C (mg Chl)$^{-1}$	–
κ_0	background attenuation coefficient	0.074	m^{-1}	from field data
κ_1	self-shading coefficient	0.0086	m^{-1} (mg Chl m^{-3})$^{-1}$	from field data
Diatoms				
$K_{P_D,I}$	half-saturation constant for irradiance	5.2	Einst m^{-2} d^{-1}	Ross et al., 1993
$K_{P_D,N}$	half-saturation constant for N	4.2	mg N m^{-3}	Ross et al., 1993
$U_{P_D,max}$	max growth rate	1.2	d^{-1}	Ross et al., 1994
v_{P_D}	sinking rate	0.5	m d^{-1}	Smayda, 1970
Q_{10,P_D}	Q_{10} coefficient	2.3	–	Eppley, 1972
θ_{0,P_D}	reference temperature	10	°C	Eppley, 1972
x_{u,P_D}	fraction of uptake excreted	0.05	–	Ross et al., 1993
x_{P_D}	fraction of biomass excreted	0.17	d^{-1}	Ross et al., 1993
Flagellates				
$K_{P_F,I}$	half-saturation constant for irradiance	5.2	Einst m^{-2} d^{-1}	Ross et al., 1993
$K_{P_F,N}$	half-saturation constant for N	2.1	mg N m^{-3}	Varela et al., 1995
$U_{P_F,max}$	max growth rate	0.96	d^{-1}	Varela et al., 1995
v_{P_F}	sinking rate	0	m d^{-1}	Smayda, 1970
Q_{10,P_F}	Q_{10} coefficient	2.3	–	Eppley, 1972
θ_{0,P_F}	reference temperature	10	°C	Eppley, 1972
x_{u,P_D}	fraction of uptake excreted	0.05	–	Ross et al., 1993
x_{P_F}	fraction of biomass excreted	0.15	d^{-1}	Varela et al., 1995

Table A2
Dissolved organic nitrogen and detritus parameters

Parameter	Description	Value	Units	Source
$Q_{10,B}$	Q_{10} coefficient	2.95	–	Baretta-Bekker et al., 1995
$\theta_{0,B}$	reference temperature	10	°C	Baretta-Bekker et al., 1995
d	DON remineralisation rate	0.20	d^{-1}	Ross et al., 1993
r	detritus remineralisation rate	0.1	d^{-1}	Andersen and Nival, 1988
v_R	detritus sinking rate	10.0	$m\ d^{-1}$	Smayda, 1970
l	non-skeletal zooplankton tissue fraction	0.95	–	Båmstedt, 1986

Table A3
Non-*Calanus* zooplankton parameters

Parameter	Description	Value	Units	Source
Q_O	N:C ratio	0.21	mg N mg C^{-1}	Båmstedt, 1986
b_O	basal metabolism coefficient	0.05	d^{-1}	Ross et al., 1994
s_O	SDA coefficient	0.51	–	Ross et al., 1994
$I_{O,\max}$	max ingestion rate	2.0	d^{-1}	Ross et al., 1994
$K_{O,F}$	half-saturation for ingestion	150	mg C m^{-3}	Ross et al., 1994
m_O	density-dependent mortality coefficient	0.10	d^{-1}	Fitted
O_{ref}	reference density for mortality	25	μg C m^{-3}	Fitted

Table A4
Calanus parameters

Parameter	Description	Value	Units	Source
m	number of age classes	80	–	–
d	width of each age class	1	d	–
q_Z	N:C ratio	0.28	mg N mg C^{-1}	Corner and O'Hara, 1986
v_0	search volume coefficient	6×10^{-5}	$m^{-3}\ d^{-1}\ \mu g\ C^{-v1}$	Hansen et al., 1990
v_1	search volume exponent	0.85	–	Marshall and Orr, 1955a
τ_0	handling time coefficient	0.64	$d\ \mu g\ C^{-1}\ \mu g\ C^{-\tau 1}$	Hansen et al., 1990
τ_1	handling time exponent	−0.80	–	Hansen et al., 1990
x_C	fractional excretion of ingested C	0.1	mg C mg C^{-1}	Assumed
x_N	fractional excretion of ingested N	0.1	mg N mg N^{-1}	Corner et al., 1965
f_C	fractional defecation of ingested C	0.2	mg C mg C^{-1}	Marshall and Orr, 1955b
f_N	fractional defecation of ingested N	0.1	mg N mg N^{-1}	Marshall and Orr, 1955b
α	N:C metabolic ratio	1.0	mg N mg C^{-1}	Assumed
β_0	basal metabolism coefficient	0.04	mg C mg C^{-1} d^{-1}	Marshall, 1973
β_S	SDA coefficient	0.1	mg C mg C^{-1}	Corner et al., 1965
γ_C	C costs of gamete production	0.1	mg C mg C^{-1}	Marshall and Orr, 1958
γ_N	N costs of gamete production	0.2	mg N mg N^{-1}	Marshall and Orr, 1958
$Q_{10,B}$	Q_{10} for basal metabolism	1.0	–	Marshall and Orr, 1958
θ_B	reference temperature for basal metabolism	12.0	°C	Marshall and Orr, 1958
ω_π	weight at 50% of assimilate to gametes	70	μg C	Carlotti et al., 1993
σ	shape factor in gamete allocation	2.0	μg C	Assumed
δ_{egg}	egg mortality	0.9	d^{-1}	Fitted
δ_{C6}	adult mortality	0.3	d^{-1}	Fitted
δ_{other}	mortality in remaining stages	0.0	d^{-1}	Fitted

Table A5
Calanus individual weight-in-stage (after Hay et al., 1991)

Stage	Weight (μg C individual^{-1})
Eggs	0.168
Nauplii	0.920
C1	1.996
C2	4.224
C3	10.100
C4	19.180
C5	47.892
C6	57.468

References

Al-Rabeh, A., 1992. Towards a general integration algorithm for time-dependent one-dimensional systems of parabolic partial differential equations using the method of lines. J. Comp. App. Math. 42, 187–198.

Andersen, V., Nival, P., 1988. A pelagic ecosystem model simulating production and sedimentation of biogenic particles: role of salps and copepods. Mar. Ecol. Prog. Ser. 44, 37–50.

Båmstedt, U., 1986. Chemical composition and energy content. In: Corner, E.D.S, O'Hara, S.C.M. (Eds.), The Biological Chemistry Marine Copepods. Clarendon Press, pp. 1–58.

Baretta, J.W., Ebenhöh, W., Ruardij, P., 1995. The European Regional Seas Ecosystem Model, a complex marine ecosystem model. Neth. J. Sea Res. 33, 233–246.

Baretta-Bekker, J.G., Baretta, J.W., Rasmussen, E.K., 1995. The microbial food web in the European Regional Seas Ecosystem Model. Neth. J. Sea Res. 33, 363–379.

Blakemore, J.S., 1987. Semiconductor Statistics. Dover Publishing, New York, 381 pp.

Bryant, A.D., Heath, M., Gurney, W.S.G., Beare, D.J. and Robertson, W., 1997. The seasonal dynamics of Calanus finmarchicus: development of a three-dimensional structured population model and application to the northern North Sea. J. Sea Res. 38, 361–379 (this issue).

Carlotti, F., Sciandra, A., 1989. Population dynamics model of *Euterpina acutifrons* (Copepoda: Harpacticoida) coupling individual growth and larval development. Mar. Ecol. Prog. Ser. 56, 225–242.

Carlotti, F., Nival, P., 1992. Model of copepod growth and development: moulting and mortality in relation to physiological processes during an individual moult cycle. Mar. Ecol. Prog. Ser. 84, 219–233.

Carlotti, F., Radach, G., 1996. Seasonal dynamics of phytoplankton and *Calanus finmarchicus* in the North Sea as revealed by a coupled one-dimensional model. Limnol. Oceanogr. 41, 522–539.

Carlotti, F., Krause, M., Radach, G., 1993. Growth and development of *Calanus finmarchicus* related to the influence of temperature: experimental results and conceptual model. Limnol. Oceanogr. 38, 1125–1134.

Corner, E.D.S., O'Hara, S.C.M. (Eds.), 1986. The Biological Chemistry of Marine Copepods. Clarendon Press, Oxford.

Corner, E.D.S., Cowey, C.B., Marshall, S.M., 1965. On the nutrition and metabolism of zooplankton III. Nitrogen excretion by *Calanus*. J. Mar. Bioll Assn. UK 45, 429–442.

Davies, A.M., 1986. Application of a spectral model to the calculation of wind drift currents in an idealised stratified sea. Cont. Shelf Res. 5, 579–610.

De Roos, A.M., 1988. Numerical methods for structured population models: the escalator boxcar train. Numeric. Meth. Part. Diff. Eqs. 4, 173–195.

Dew, P.M., Walsh, J.E., 1981. A set of library routines for solving parabolic equations in one space variable. ACM Trans. Math. Software 7, 295–314.

Dooley, H.D., 1981. The role of axially varying vertical mixing along the path of a current in generating phytoplankton blooms. Phil. Trans. R. Soc. A 302, 649–660.

Dooley, H.D., 1983. Seasonal variability in the position and strength of the Fair Isle Current. In: Sundermann, J., Lenz, W. (Eds.), Proceedings of the Symposium on North Sea Dyanamics, Hamburg, September 1981. Springer-Verlag, Berlin, pp. 108–119.

Eppley, R.W., 1972. Temperature and phytoplankton growth in the sea. Fish. Bull. 70, 1063–1085.

Garrett, C.J.R., Loder, J.W., 1981. Dynamical aspects of shallow sea fronts. Phil. Trans. R. Soc. A 302, 562–581.

Gear, C.W., 1971. Numerical Initial Value Problems in Ordinary Differential Equations. Section 11.1 — Stiff Equations. Prentice-Hall Series in Automatic Computation. Prentice-Hall, New Jersey.

Hansen, B., Tande, K.S., Berggreen, U.C., 1990. On the trophic fate of *Phaeocystis pouchetii* (Hariot). III. Functional response in grazing demonstrated on juvenile stages of *Calanus finmarchicus* (Copepoda) fed diatoms and *Phaeocystis*. J. Plankt. Res. 12, 1173–1187.

Hay, S.J., 1995. Egg production and secondary production of common North Sea copepods: field estimates with regional and seasonal comparisons. ICES J. Mar. Sci. 52, 315–327.

Hay, S.J., Kiørboe, T., Matthews, A., 1991. Zooplankton biomass and production in the North Sea during the Autumn Circulation Experiment, October 1987–March 1988. Cont. Shelf Res. 11, 1453–1476.

Henderson, E.W., Steele, J.H., 1995. Comparing models and observations of shelf plankton. J. Plankt. Res. 17, 1679–1692.

Henderson, E.W., Steele, J.H., 1996. A shelf plankton model: description and testing. Scottish Fisheries Research Report 57, 14 pp.

Holligan, P.M., 1981. Biological implications of fronts on the northwest European shelf. Phil. Trans. R. Soc. A 302, 547–562.

Horne, E.P.W., Loder, J.W., Harrison, W.G., Mohn, R., Lewis, M.R., Irwin, B., Platt, T., 1989. Nitrate supply and demand ant the Georges Bank tidal front. Sci. Mar. 53, 145–158.

Joint, I.R., 1987. Physiological ecology of picoplankton in various oceanographic provinces. In: Platt, T., Li, W.K.W. (Eds.), Photosynthetic Picoplankton. Can. Bull. Fish. Aquat. Sci. 214, 287–309.

Kiørboe, T., Møhlenberg, F., Hamburger, K., 1985. Bioenergetics of the planktonic copepod *Acartia tonsa*: relation between

feeding, egg production and respiration, and composition of specific dynamic action. Mar. Ecol. Prog. Ser. 26, 85–97.

Le Fevre, J., 1986. Aspects of the biology of frontal systems. Adv. Mar. Biol. 23, 163–299.

Mann, K.H., Lazier, J.R.N., 1991. Dynamics of Marine Ecosystems. Biological–Physical Interactions in the Oceans. Blackwell, Boston, 466 pp.

Marshall, S.M., 1973. Respiration and feeding in copepods. In: Russel, F., Yonge, M. (Eds.), Adv. Mar. Biol. 11, 57–120.

Marshall, S.M., Orr, A.P., 1955a. Experimental feeding of the copepod *Calanus finmarchicus* (Gunner) on phytoplankton cultures labelled with radioactive carbon (^{14}C). Deep Sea Res. 3, 110–114.

Marshall, S.M., Orr, A.P., 1955b. On the biology of *Calanus finmarchicus*. VIII. Food uptake, assimilation and excretion in adult and stage V *Calanus*. J. Mar. Biol. Assn. UK 34, 495–529.

Marshall, S.M., Orr, A.P., 1958. On the biology of *Calanus finmarchicus*. X. Seasonal changes in oxygen consumption. J. Mar. Biol. Assn. UK 37, 459–472.

Miller, C.B., Tande, K.S., 1993. Stage duration estimation for *Calanus* populations, a modelling study. Mar. Ecol. Prog. Ser. 102, 15–34.

Pätsch, J., 1994. MOCADOB a model generating synthetical time series of solar radiation for the North Sea. Ozeanographie 16, 67 pp.

Pederson, G., Tande, K.S., 1992. Physiological plasticity to temperature in *Calanus finmarchicus*. Reality or artefact?. J. Exp. Mar. Biol. Ecol. 155, 183–197.

Pingree, R.D., Griffiths, D.K., 1978. Tidal fronts on the shelf seas around the British Isles. J. Geophys. Res. 83, 4615–4622.

Pingree, R.D., Holligan, P.M., Mardell, G.T., 1978. The effects of vertical stability on phytoplankton distributions in the summer on the north west European shelf. Deep Sea Res. 25, 1011–1028.

Planque, B., Fromentin, J., 1996. *Calanus* and environment in the eastern North Atlantic. I. Spatial and temporal patterns of *C. finmarchicus* and *C. helgolandicus*. Mar. Ecol. Prog. Ser. 134, 101–109.

Pohlmann, T., 1996a. Predicting the thermocline in a circulation model of the North Sea — Part I: model description, calibration and verification. Cont. Shelf Res. 16, 131–146.

Pohlmann, T., 1996b. Calculating the annual cycle of the vertical eddy viscosity in the North Sea with a three-dimensional baroclinic shelf sea circulation model. Cont. Shelf Res. 16, 147–162.

Pohlmann, T., 1996c. Calculating the development of the thermal vertical stratification in the North sea with a three-dimensional baroclinic circulation model. Cont. Shelf Res. 16, 163–194.

Pohlmann, T., 1996d. Simulating the heat storage in the North sea with a three-dimensional circulation model. Cont. Shelf Res. 16, 195–213.

Riemann, B., Simonsen, P., Stensgaard, L., 1989. The carbon and chlorophyll content of phytoplankton from various nutrient regimes. J. Plankt. Res. 11, 1037–1045.

Ross, A.H., Gurney, W.S.C., Heath, M.R., Hay, S.J., Henderson, E.W., 1993. A strategic simulation model of a fjord ecosystem. Limnol. Oceanogr. 38, 128–153.

Ross, A.H., Gurney, W.S.C., Heath, M.R., 1994. A comparative study of the ecosystem dynamics of four fjords. Limnol. Oceanogr. 39, 318–343.

Simpson, J.H., Hunter, J.R., 1974. Fronts in the Irish Sea. Nature 250, 404–406.

Smayda, T.J., 1970. The suspension and sinking of phytoplankton in the sea. Oceanogr. Mar. Biol. Ann. Rev. 8, 353–414.

Soulsby, R.L., 1990. Tidal current boundary layers. In: Le Mehaute, B., Hanes, D.M. (Eds.), The Sea. Wiley, New York, pp. 523–566.

Steele, J.H., Henderson, E.W., 1993. The significance of interannual variability. In: Evans, G.T., Fasham, M.J.R. (Eds.), Towards a Model of Ocean Biogeochemical processes. Springer-Verlag, New York, pp. 237–260.

Steele, J.H., Henderson, E.W., 1995. Predation control of plankton demography. ICES J. Mar. Sci. 52, 565–573.

Tett, P., Edwards, A., Jones, K., 1986. A model for the growth of shelf sea phytoplankton in summer. Estuar. Coast. Shelf Sci. 23, 641–672.

Thompson, B.M., 1982. Growth and development of *Pseudocalanus elongatus* and *Calanus* sp. in the laboratory. J. Mar. Biol. Assn. UK 62, 359–372.

Turrell, W.R., Henderson, E.W., Slesser, G., 1990. Residual transport within the Fair Isle Current observed during the Autumn Circulation Experiment (ACE). Cont. Shelf Res. 10, 521–543.

Varela, R.A., Cruzado, A., Gabaldón, J.E., 1995. Modelling primary production in the North Sea using ERSEM. Neth. J. Sea Res. 33, 337–361.

Williams, R., 1985. Vertical distributions of *Calanus finmarchicus* and *C. helgolandicus* in relation to development of the seasonal thermocline in the Celtic Sea. Mar. Biol. 86, 145–149.

Wolf, K.U., Woods, J.D., 1988. Lagrangian simulation of primary production in the physical environment — the deep chlorophyll maximum. Towards a theory of biological–physical interactions in the world ocean. Kluwer, Dordrecht, pp. 51–70.

Wood, S.N., Nisbet, R.M., 1991. Estimation of mortality rates in stage-structured populations. Volume 90 of Lecture Notes in Biomathematics.

Wood, B.J.B., Tett, P.B., Edwards, A., 1973. An introduction to the phytoplankton, primary production and relevant hydrography of Loch Etive. J. Ecol. 61, 569–585.

Woods, J.D., Onken, R., 1982. Diurnal variation and primary production in the ocean — preliminary results of a Lagrangian ensemble model. J. Plankt. Res. 4, 735–756.

Woods, J.D., Barkmann, W., 1995. Modelling oligotrophic zooplankton production: seasonal oligotrophy off the Azores. ICES J. Mar. Sci. 52, 723–734.